

1 **REVISION 2**

2

3 **TOURMALINE AS A PETROGENETIC MONITOR OF THE ORIGIN AND**
4 **EVOLUTION OF THE BERRY-HAVEY PEGMATITE (MAINE, USA)**

5 Roda-Robles, Encarnación ^{1§}, Simmons, William ², Pesquera, Alfonso ¹,
6 Gil-Crespo, Pedro P. ¹, Nizamoff, James ², Torres-Ruiz, José ³

7 ¹*Dpt. Mineralogía y Petrología, UPV/EHU, Bilbao, Spain, §encar.roda@ehu.es*

8 ²*Dpt. Earth & Env. Sci, Univ. New Orleans, New Orleans, LA, USA*

9 ³*Dpt. Mineralogía y Petrología, Universidad de Granada, Spain*

10

11 *Key words:* tourmaline, pegmatites, mineral chemistry, Maine, USA

12

13 **ABSTRACT**

14 The Berry-Havey pegmatite (Oxford pegmatite field, Androscoggin County, Maine,
15 USA), enriched in Li, F, B, Be and P, is intruded in hornblende-rich amphibolite, with
16 minor biotite or diopside. The pegmatite has a complex internal structure, with four
17 texturally and compositionally different zones, which show an increasing degree of
18 evolution inward: wall zone, intermediate zone, core margin and core zone. The main
19 minerals are quartz, feldspars, Al-micas, tourmaline, with minor Fe-micas, garnet, beryl,
20 amblygonite-montebrazite, Fe-Mn phosphates and apatite. Tourmaline is present in all
21 zones of the pegmatite, showing different textures: black anhedral crystals in the wall
22 and intermediate zones; black prisms of up to 40 cm in length in the intermediate zone;
23 black tapered prisms, surrounded by a pseudo-graphic intergrowth of quartz or albite
24 with black ± green/bluish tourmaline, and constituting a continuous layer under the core
25 zone; multicolored and “watermelon” zoned crystals in the core zone; and gemmy deep
26 green and color-zoned “watermelon” tourmaline prisms, up to 15 cm length, inside the
27 pockets. A complete chemical evolution from Mg-rich schorl in the wall zone to elbaite
28 with an important deprotonation in the pockets inside the core zone is observed. The
29 most plausible exchange vectors for this chemical evolution are FeMg_{-1} ,
30 ${}^Y\text{Al}^W\text{O}({}^Y\text{R}^{2+W}(\text{OH}))_{-1}$ and $\text{Al}[\text{X}]^X(\text{R}^{2+}\text{Na})_{-1}$, (where $\text{R}^{2+} = \text{Fe}^{2+} + \text{Mg}^{2+} + \text{Mn}^{2+} + \text{Zn}^{2+}$),
31 for the tourmalines from the wall and intermediate zones. In the core margin tourmaline
32 composition evolves from schorl toward Li-rich species through the substitution
33 (${}^Y\text{Al}^Y\text{Li}^Y\text{R}^{2+}_{-2}$). Later, during the crystallization of the core zone, this exchange vector
34 combined with the substitution ($[\text{X}]^Y\text{Al}_{0.5}^X\text{Na}_{-1}^Y\text{Li}_{0.5}$). Finally, the gemmy tourmalines
35 from the pockets show a deprotonation related to the exchange vector ${}^Y\text{Al}^W\text{O}_2{}^Y\text{Li}$.

36 $\text{Al}^{\text{IV}}(\text{OH})_2$, and may be classified as darrellhenryite. These substitutions may reflect an
37 increase in oxygen fugacity, and a decrease in Li and F related to the crystallization of
38 lepidolite and amblygonite-montebrazite in the core zone adjacent to or within the
39 pockets. The crystallization of these minerals would reduce the availability of Li and F
40 for the very latest tourmaline crystals, growing inside the pockets, where the
41 deprotonation becomes important. Chemical and textural variation in tourmaline is
42 consistent with a fractional crystallization process for the internal evolution of the
43 Berry-Havey pegmatite. Crystallization of the tourmaline layer under the core zone may
44 be related to the exsolution of the fluid phase implied in the formation of pockets.

45

46

Introduction

47 Pegmatites are common in the Central Maine Belt of the United States. Many of them
48 are barren bodies, however, rare-element-bearing pegmatites, showing a well developed
49 internal zoning, are also widespread in this region. The Berry-Havey pegmatite
50 (Androscoggin County, Maine, USA), is a highly evolved, rare-element pegmatite
51 enriched in Li, F, B, Be and P. It belongs to the Oxford pegmatite field, located in the
52 western portion of the state of Maine, within the Sebago migmatite terraine (Solar and
53 Tomascak, 2009). In this field, pegmatites have been mined for more than a century for
54 gem tourmaline. The first gem tourmaline was discovered at this pegmatite in 1910.
55 Tourmaline occurs in all pegmatite zones and shows a continuous and well-defined
56 chemical evolution from the outer to the inner zones. Previous studies of pegmatitic
57 tourmaline have shown the relationship of tourmaline chemistry to the evolution of the
58 host pegmatite. (e.g. Jolliff et al. 1986; Selway et al. 1999; Roda et al. 1995; Keller et
59 al. 1999; Novak, 2000; Tindle et al. 2002; Roda-Robles et al, 2004, 2011). This study
60 investigates the relationship of tourmaline chemistry of the Berry-Havey pegmatite to
61 help decipher the petrogenesis of the Berry-Havey pegmatite, and contribute to the
62 understanding of other pegmatites in the Oxford field that share some features with this
63 pegmatite.

64 This study deals mainly with the paragenesis, textural characteristics and
65 compositional variation of tourmaline in the different zones of the Berry-Havey
66 pegmatite. The possible substitution mechanisms accounting for the compositional
67 variation of tourmaline are discussed on the basis of the analytical results. Finally, the

68 implications of the chemical and textural variability of tourmaline across the pegmatite
69 for the internal evolution of this body are also evaluated.

70

71

Geological Setting

72 The Berry-Havey pegmatite belongs to the Oxford pegmatite field, where pegmatites
73 concentrate along the northwest, northeast and eastern margins of the Sebago Migmatite
74 Domain (SMD), previously mapped as the Sebago Batholith (SB) (Fig. 1). Different
75 degrees of evolution are attained by pegmatites in this region, with an internal zonation
76 that varies from poor to well developed, sometimes with the occurrence of pockets,
77 where gem tourmaline may be present. The Berry-Havey pegmatite occurs at the
78 northeast limit of the SMD. This Domain, described by Solar and Tomascak (2009),
79 mainly consists of pelitic migmatite and diatexite with subordinate centimeter- to meter-
80 scale bodies of foliated granite layers, subconcordant with host rock structures. The
81 SMD rocks are cut by centimeter-scale granite dikes of similar composition and texture
82 as the SB rocks (Solar and Tomascak 2009). Pegmatitic and aplitic units are also
83 commonly observed in this domain. The SMD surrounds the Sebago batholith as
84 previously mapped (Osberg et al, 1985). Later work by Tomascak et al. (1996a) and
85 Solar and Tomascak (2001), separated this batholith into a granite pluton (the Sebago
86 pluton, “sensu stricto”) and the SMD that underlies the remaining area of Oxford
87 County (Solar and Tomascak 2009). Both, the extensive SMD and the Sebago pluton,
88 belong to the Central Maine Belt (CMB), of the northern Appalachians (Fig. 1), a
89 prominent NE-SW trending unit that occupies most of New England and New
90 Brunswick, Canada, and that is composed of a Lower Paleozoic sedimentary succession
91 that was intruded by Devonian to Permian igneous rocks (e. g. Osberg 1978; Williams
92 1978; Solar and Brown 2001a). In the CMB the metamorphic facies change from
93 greenschist in the northeast to upper amphibolite facies (and migmatite) to the
94 southwest (Guidotti 1989; 1993) (Fig. 1). Migmatites of the SMD in Maine and New
95 Hampshire, are the core of a diachronous “metamorphic high”, in which the protolith is
96 interpreted to be rocks of the CMB stratigraphic sequence (Solar and Brown 2001b;
97 Johnson et al. 2003). According to structural, geochemical and geochronological data,
98 some authors propose that in the CMB pluton emplacement was syntectonic with
99 respect to the Acadian orogeny (see Brown and Solar 1998a; 1998b; 1999, Solar &
100 Tomascak 2009, among others). However, some plutons cut across the regional
101 structures without any structural trend or a significant deformation aureole (Brown and

102 Solar 1999), which is interpreted by other authors (e.g. De Yoreo et al. 1991) as
103 illustrative of a post-tectonic character of those plutons. Geochronological data on the
104 Sebago pluton give ages of 293 Ma (U-Pb TIMS in monazite, Tomascak et al. 1996b).
105 The relationships between the Sebago pluton and the SMD are still undefined. It seems
106 clear that the pluton has intruded into country rocks belonging to the SMD. According
107 to the age calculated for the deformation presented by the rocks in the SMD and the age
108 of the SB, the difference in the age between them could be around 100 Ma, which could
109 indicate that the Sebago pluton and the SMD are unrelated and just fortuitously located
110 (Solar and Tomascak 2009).

111

112 **Field relationships and petrography of the pegmatitic body**

113 With the present exposure of the Berry-Havey pegmatite it is not easy to determine the
114 shape of the pegmatite, or its internal structure. A straight contact is observed in the
115 southern limit of the open pit. To the east, the contact becomes more irregular, with a
116 few dike-like branches that cross-cut the country rock. In the rest of the quarry it is not
117 possible to observe the contact (Fig. 2). To the southwest of the quarry, the pegmatite is
118 conformable to the foliation of the host rock, with a dip close to 40° SSE, whereas in the
119 northern part of the exposure the body seems to be more horizontal. The country rock is
120 not homogeneous. Much of the material from the southern contact is hornblende-rich
121 amphibolite, with minor biotite or diopside in places. Locally, the host rock at the
122 contact is extremely rich in biotite. The samples of tourmaline analyzed from the wall
123 zone were taken in those areas close to the amphibolite, that is the most common facies
124 in the country rock. This country rock does not show any local metasomatism.
125 Moreover, the development of tourmaline-enriched zones in the contact zone has not
126 been observed.

127 The pegmatite shows a well-developed complex internal structure. Based on spatial
128 distribution, paragenesis, textural features, and chemical composition, four different
129 zones have been distinguished: wall zone, intermediate zone, core margin and core zone
130 (Fig. 2, Table 1). These zones are subparallel to the country rock, with quite irregular
131 boundaries, particularly along the core-margin-core zone transition. From the contact
132 with the host rock to the core of the pegmatite, the following sequence is observed:

133 (1) The wall zone (WZ), only observed at the southern part of the quarry, is
134 immediately in contact with the country rock. Texturally it is the most homogeneous
135 zone observed in the pegmatite, commonly with a pegmatitic texture with very fine- to
136 medium-sized crystals. Locally, it may present a gneissic texture. The main minerals are
137 quartz, plagioclase, K-feldspar that locally exhibits a light greenish color, biotite and
138 muscovite, with tourmaline and garnet as common minor phases, and accessory apatite.

139 (2) The intermediate zone (IZ) is volumetrically the most important, constituting
140 approximately 58 % of the outcrop. More than 85 % of the volume of the IZ consists of
141 graphic intergrowths of quartz-K-feldspar and less abundant quartz-plagioclase. Other
142 minor minerals are biotite, garnet and black tourmaline, which appear scattered inside
143 the graphic-granite masses, as fine- to medium-sized crystals. The IZ is localized at both
144 sides of the core zone/core-margin. In the upper half of the body, it constitutes a quite
145 tabular unit, underlying the WZ, over the core zone/core-margin, with ~5 m thickness
146 (Fig. 2). At the lower part of the pegmatite the IZ is volumetrically more important and
147 more irregular in shape and thickness. (Fig. 2). In this lower part of the IZ, on the
148 northern side of the quarry, the texture and mineralogy change locally in two outcrops
149 (Fig. 2). Main minerals there are quartz, K-feldspar and black tourmaline. Textures are
150 clearly different from those observed in the rest of the IZ. Graphic intergrowths of
151 quartz and K-feldspar are absent and these two minerals occur as coarse, locally blocky
152 crystals. Tourmaline grain size is also much coarser, with prismatic crystals up to 40 cm
153 in length. The volumetrically more abundant unit, with the quartz-K-feldspar graphic
154 intergrowth, is designated IZ-I; the other one, with the blocky quartz and K-feldspar,
155 and the large prismatic tourmaline crystals, is designated IZ-II.

156 (3) The volumetrically important core margin (CM), (\approx 32% of the outcrop), is
157 located between the two units of the IZ, closer to the hanging wall than to the foot wall,
158 which is below the surface of exposure (Fig. 2). The CM zone hosts the different pods
159 that constitute the core of the pegmatite. The CM consists of albite (clevalandite) and
160 quartz, but is more mineralogically and texturally complex than the intermediate zone.
161 Tourmaline appears as black, coarse prisms, crowned by an intergrowth of black \pm
162 green/bluish tourmaline, albite and quartz, giving rise to a quite continuous layer just
163 below the core pods. Garnet occurs as medium sized reddish-brownish crystals,
164 concentrated in a discontinuous layer just below the tourmaline level. This garnet layer

165 is used by miners in this area of Maine as a guide while searching for pockets, as they
166 are rarely found below the layer.

167 (4) The core zone (CZ) represents the innermost zone of the pegmatite, which is the
168 most complex zone, not only because of its mineralogy, but also because of its textures.
169 It is not a continuous unit, but consists of pods of different sizes hosted by the CM (Fig.
170 2). The pods are commonly isolated but in places may be interconnected. The size of
171 these pods ranges from a couple of meters to ~10 meters across and may contain meter-
172 sized pockets (miarolitic cavities). The main minerals in the pods are blocky quartz and
173 K-feldspar, in contact with irregular masses of fine-grained grayish to purple lepidolite,
174 book muscovite \pm lepidolite, albite, greenish and pinkish tourmaline, whitish to pinkish
175 coarse beryl crystals and amblygonite-montebasite- or Fe-Mn-phosphates in sub-
176 rounded nodules. Cassiterite and Nb-Ta oxides are the main accessory minerals. Inside
177 the pockets the main minerals are smoky quartz, albite, lepidolite, hydroxylherderite,
178 cassiterite, beryl, and green and “watermelon” gemmy tourmaline. Clay minerals also
179 occur frequently, usually appearing among the quartz crystals, being the matrix where
180 many of the gemmy tourmaline prisms are found.

181

182

Textural characteristics of tourmaline

183 Tourmaline occurs in all zones of the pegmatite, with important textural and
184 compositional variations among the different zones (Table 1). In the WZ, tourmaline is
185 scarce, occurring as very fine to fine-grained, an- to subhedral, prismatic, black crystals,
186 together with quartz, feldspars, muscovite, garnet and biotite. Under the microscope
187 tourmaline from the WZ exhibits strong brownish colors, commonly more orange in the
188 border and more greenish in the cores of the crystals, with moderate pleochroism in
189 both cases. In backscattered electron (BSE) images, tourmaline from the WZ is mostly
190 homogeneous. However, some tourmaline crystals display a marked heterogeneity, with
191 successive overgrowths, with finger-like shapes pointing toward the inner parts of the
192 pegmatite (Fig. 3a). The contacts between zones of different colors are, in general,
193 straight and well defined, except in some interior zones of the crystals, which look
194 partially embayed.

195 The IZ-I is characterized by the abundance of graphic intergrowths of quartz and K-
196 feldspar, with tourmaline occurring as a minor constituent. It appears as black, sub-
197 anhedral, fine-grained crystals, and in places is graphically intergrown with quartz.

198 Under the microscope the color of tourmaline from the IZ and from the WZ are clearly
199 different. In the IZ most of the crystals are blue, darker in the rims than in the cores, and
200 with a slight pleochroism. Tourmaline from the IZ-I is mostly homogeneous as
201 evidenced from BSE images. Some crystals are partially rimmed by discontinuous
202 concentric thin zones of different brightness (Fig. 3b). In the IZ-II the quartz-K-feldspar
203 graphic intergrowths are scarce, whereas schorl may be very abundant, appearing as
204 black, prismatic crystals up to 6 x 40 cm (Fig. 4a). Under the microscope, crystals show
205 a concentric chromatic zoning, following the same pattern observed in tourmalines from
206 the IZ-I, that is, dark bluish rims and lighter bluish cores, with a slight pleochroism in
207 the both cases. In the BSE images these prisms appear homogeneous.

208 In the CM tourmaline is also quite abundant. Many crystals occur as tapered black
209 prisms growing perpendicular to the pegmatite contacts that increase in width in the
210 direction of the core of the pegmatite. The most common size of these prisms is ~ 50 cm
211 in length, and up to ~ 15 cm in diameter. The thick ends of most crystals are crowned
212 by black ± green/bluish tourmaline, intergrown with quartz ± albite (cleavelandite),
213 giving a graphic texture (Fig. 4b). Less commonly, tourmaline crystals are broken,
214 giving rise to a “puzzle” structure inside a matrix of quartz and albite. Under the
215 microscope, the color of tourmaline from the CM is generally lighter than in the
216 previous zones. Black tourmaline in hand sample, under the microscope appears as
217 bluish crystals in the core and colorless or light bluish in the rim, with a strong
218 pleochroism in both cases, from bluish to colorless. No systematic change of color was
219 observed along the c-axis of these crystals. In the BSE images, the tourmaline prisms
220 from the CM show a homogeneous core, surrounded by a concentric rim with a
221 different color, showing a straight, well defined limit between core and rim (Fig. 3c).
222 Overgrowing this rim, it is not uncommon to observe a much thinner, darker, frayed
223 edge of tourmaline (Fig. 3c).

224 In the case of the crowns surrounding the tourmaline prisms in the CM, the greenish
225 and bluish crystals in hand sample are generally colorless under the microscope,
226 although in some cases they exhibit a very light greenish or bluish shade. The transition
227 from black to colored tourmaline is sharp in hand samples (Fig. 4c) and in thin sections.
228 However, BSE images reveal that the chemical zonation corresponding to the color
229 zones is not always so sharp. Whereas the darkest zones in hand sample, in BSE are
230 quite homogeneous in the core of the crystals, close to the greenish areas the color is
231 changing, with darker shades of irregular distribution, and an irregular limit between the

232 black and green areas (Fig. 3d). The greenish parts of the crystals are heterogeneous,
233 showing patchy zoning or cellular textures in the inner zones of the crystals, which are
234 overgrown by darker rims, which could suggest cycles of stabilization and
235 destabilization (Fig. 3d).

236 Tourmaline is an important mineral in the CZ. It occurs with different colors and
237 textures. Abundant greenish, fine-to-medium-grained tourmaline prisms are associated
238 with medium-to-coarse book crystals of muscovite. Small pinkish tourmaline crystals
239 occur inside the fine-grained lepidolite masses. Prismatic crystals of watermelon
240 tourmaline, up to 15 cm in length, with pinkish cores and greenish rims, have also been
241 observed in this zone, most being partially replaced by clay minerals. Moreover, radial
242 prisms, up to 20 cm in length, of multicolored tourmaline embedded in feldspars and
243 quartz are also abundant (Fig. 4d). Many of these crystals are extensively replaced by
244 clay minerals. Another textural variety, observed rarely in the pods from the CZ,
245 corresponds to transparent greenish prismatic crystals of tourmaline found inside the
246 amblygonite-montebasite nodules. Numerous pockets hosted by the pods of the CZ
247 contain mainly euhedral to subhedral greenish and rarer pink to watermelon gem-
248 quality tourmaline. (Fig. 4e). The size of these crystals is generally under 4 cm in
249 length, but rarely crystals of up to 15 cm have been found. Under the microscope these
250 crystals, included in the pods and pockets, are colorless to light greenish in color with
251 slight pleochroism.

252 In addition to the tourmaline from all the zones inside the main body of the Berry-
253 Havey pegmatite, tourmaline crystals from a vertical pegmatitic “branch”, with a
254 thickness < 50 cm, occurring at the southern contact of the pegmatite, have been
255 studied. This tourmaline occurs as fine, black crystals that under the microscope exhibit
256 strong brownish to orange colors in the border and more greenish color in the core,
257 similar to those from the WZ of the pegmatite. In the BSE images some crystals reflect
258 a complex crystallizing history, including more than one tiny nucleus that appears
259 overgrown by lighter zones. This feature may account for coalescence of small grains
260 mantled by outer zones with a very irregular shape, and also suggests cycles of
261 stabilization and destabilization to generate these types of textures. (Fig. 3e).

262

263 **Sampling and Analytical methods**

264 Tourmaline crystals were taken from all the zones of the Berry-Havey pegmatite,
265 including all the different textural varieties of tourmaline occurring in the CM and CZ.

266 Close to 200 thin sections were made to study the tourmaline petrography under the
267 microscope. Close to 1000 microprobe analyses were carried out on representative
268 tourmaline samples from the different zones of the pegmatite, at the University of
269 Granada (Spain) and at the University Paul Sabatier (Toulouse, France), using in both
270 cases a Cameca SX50 microprobe equipped with four wavelength-dispersive
271 spectrometers. Operating conditions were 20 kV accelerating voltage, 20 nA beam
272 current, and a beam diameter of about 2 μm . Both natural and synthetic standards were
273 used: natural fluorite (F), natural sanidine (K), natural pollucite (Cs), synthetic MnTiO_3
274 (Ti, Mn), natural diopside (Ca), synthetic BaSO_4 (Ba), synthetic Fe_2O_3 (Fe), natural
275 albite (Na), natural periclase (Mg), synthetic SiO_2 (Si), natural apatite (P), natural
276 sphalerite (Zn), synthetic Cr_2O_3 (Cr) and synthetic Al_2O_3 (Al). Data were reduced using
277 the procedure of Pouchou and Pichoir (1985). Analytical errors are estimated to be on
278 the order of $\pm 1\text{-}2\%$ (relative) for major elements and $\pm 10\%$ for minor elements.

279 Close to 130 LA-ICP-MS analyses were made on representative tourmaline samples
280 from the different zones of the pegmatite. All these analyses were performed on
281 samples already analyzed by electron-microprobe for major and minor elements. These
282 analyses were conducted with a 213 nm Mercantek Nd-YAG laser coupled to an
283 Agilent 7500 ICP-MS with a shielded plasma torch, using the NIST-610 glass as
284 standard. The ablation was carried out in a He atmosphere. The laser beam was fixed to
285 a 95 microns wide square section. The spot was pre-ablated for 45 seconds using a laser
286 repetition rate of 10 Hz and 40% output energy. Then the spot was ablated for 60
287 seconds at 10 Hz with a laser output energy of 75%. To keep the laser focused during
288 ablation, the sample stage was set to move upwards 5 mm every 20 seconds. A typical
289 session of analysis of a single thin section began and ended with the analysis of the
290 NIST-610 glass (about 450 ppb of each element), which was also analyzed every nine
291 spots to correct for drift. Silicon was used as internal standard. Data reduction was
292 carried out with a custom software (freeware available from F. Bea) of the STATA
293 commercial package. This software permits identification and elimination of outliers,
294 blank subtraction, drift correction, internal standard correction and conversion to
295 concentration units. The precision, calculated on the five to seven replicates of the
296 NIST-610 measured in every session, is in the range $\pm 3\%$ to $\pm 7\%$ for most elements. In
297 conditions described, detection limits calculated by measuring five replicates of a large
298 and homogeneous crystal of astrophyllite, ranged from better than 0.01 ppm for REE,
299 Y, Th and U, to about 0.5 ppm for Li.

300 Structural formulae of tourmaline that were analyzed for Li by Laser Ablation were
301 normalized on 15 cations exclusive of B, Ca, Na and K (Henry and Dutrow 1996). The
302 Li contents of tourmaline crystals that were not analyzed by Laser Ablation, and where
303 MgO is < 1.25 wt.% were calculated on the basis of 6 Si apfu, by using the equation Li
304 (apfu) = $3 - \Sigma Y$. The amount of B₂O₃ corresponding to three boron cations in the
305 structural formula was calculated from stoichiometric constraints. In those samples
306 where MgO values were >1.25 wt.%, Li₂O was assumed as zero.

307

308

309

Results and discussion

310

Chemical composition of tourmalines

311

312

313

314

315

316

317

318

319

320

321

322

323

324

325

326

327

328

329

330

331

332

333

Results of representative electron-microprobe analyses obtained on tourmaline samples from every zone are listed in Table 2. Most of the analyzed tourmalines are alkali tourmalines according to the nomenclature of Henry et al. (2011) (Fig. 5a), with a wide variation in the vacancies content. Tourmalines from the WZ, IZ-I and IZ-II, as well as the black tourmalines from the CM and some colored ones, mostly belong to the alkali subgroup 1 of the (Na+K)-R²⁺ species (Fig. 5b). There are also some X-site vacancy-rich crystals, probably foitites; and a few analyses belong to the alkali subgroup 4 and others to the alkali subgroup 3 (Table 2). The rest of the colored tourmaline crystals from the CM and all the tourmalines from the CZ belong to the alkali subgroup 2 of the (Na+K)-Li species (Fig. 5b). Tourmaline structural formulae are given in Table 2. Most of the analyses of the tourmalines from the WZ, IZ-I and IZ-II seem to be consistent with dravite, oxy-dravite, schorl, oxy-schorl, and a few foitites. (Table 2); whereas the composition of most of the tourmalines associated with the CM and CZ correspond to schorl, oxy-schorl, fluor-schorl, elbaite, fluor-elbaite, darrellhenryite, and rossmanite; schorl being the dominant component in the black crystals and elbaite in the colored ones (Table 2). The chemical composition of tourmaline evolved through the following sequence from the WZ to the pockets inside the CZ (Table 2, Fig. 5c): (1) tourmalines from the WZ are intermediate between schorl and dravite, generally with a higher schorl content (0.98-1.89 apfu Fe²⁺), and often with important vacancy content (< 0.30 X-site vacancies pfu); (2) in the IZ, schorl is the dominant tourmaline component (1.55-2.28 apfu Fe²⁺), with a high content in the foitite component (0.20-0.54 X-site vacancies pfu); (3) in the CM tourmaline composition changes from vacancy-rich schorl (< 2.29 apfu Fe²⁺ and < 0.51 X-site vacancies pfu) to Fe-rich elbaite (< 0.33 apfu Fe²⁺), often

334 with a significant rossmanite content (< 0.36 X-site vacancies pfu). The Li content
335 increases from the black to the greenish and bluish crystals; (4) in the CZ all the
336 tourmalines are elbaïtes ($0.00\text{-}0.43$ apfu Fe^{2+}) with a high rossmanite content ($0.20\text{-}0.63$
337 X-site vacancies pfu). In addition, some gemmy elbaïte crystals from the pockets show
338 a significant deprotonation and high vacancy content ($0.29\text{-}0.48$ X-site vacancies pfu),
339 being classified as darrellhenryite.

340 Overall, the tourmaline samples show proportionally large variations for SiO_2
341 ($34.32\text{-}39.78$ wt%), Al_2O_3 ($29.63\text{-}43.98$ wt%), FeO ($0.00\text{-}15.18$ wt%), MgO ($0.00\text{-}5.95$
342 wt%), Li_2O ($0.01\text{-}2.58$ wt%), TiO_2 ($0.00\text{-}1.46$ wt%), Na_2O ($1.24\text{-}2.85$ wt%), MnO
343 ($0.00\text{-}1.54$ wt%), and F ($0.00\text{-}1.79$ wt%). Smaller variations are observed for ZnO
344 ($0.00\text{-}1.05$ wt%), CaO ($0.00\text{-}0.86$ wt%), and K_2O ($0.00\text{-}0.24$ wt%). The contents of Cl
345 are below the detection limit of the microprobe, whereas the F content changes in a
346 broad range (Fig. 5d). The tourmalines analyzed from the WZ, IZ-I and IZ-II show F
347 contents lower than 0.5 apfu (Table 2, Fig. 5d). Most of the black tourmaline crystals
348 from the CM are similarly F-poor. However, some black crystals and most of the
349 greenish and bluish ones may be classified as fluor-tourmalines (Table 2, Fig. 5d). In
350 the case of the tourmaline from the CZ, more than a half of the analyses are F-rich
351 (Table 2, Fig. 5d). Some of the analyzed crystals belong to the oxy-species, mainly in
352 those from the WZ, IZ and CZ (Table. 2).

353 Concentrations in trace elements in the tourmalines from the Berry-Havey are in
354 general quite low, except for Zn, as is usual in tourmalines associated to pegmatites
355 (Roda et al. 1995; Roda-Robles et al. 2012) (Table 3, Fig. 6). The highest contents in
356 Sc, Sr and LREE correspond to the tourmalines from the wall zone, and are interpreted
357 as being the result of the influence of the amphibolites of the country rock. Manganese,
358 Nb, Ta and Sn show a slight increase from the wall zone toward the core, with a final
359 decrease in the pockets, probably due to the crystallization of Nb-Ta-oxides, cassiterite
360 and Mn-rich phosphates in the pods of the CZ, that would have significantly depleted
361 the concentrations of these elements in the remaining melt. Beryllium behaves in the
362 same way, with a final depletion in the tourmalines from the pockets, which similarly
363 may be explained by the crystallization of beryl crystals in the pods of the CZ. The
364 highest contents in HREE occur in the gemmy tourmaline from the pockets, probably
365 due to the fractionation of the LREE during pegmatitic internal evolution, with the
366 heavy rare earths concentrated until the end of the crystallization.

367

368 **Substitution schemes**

369 In order to evaluate the substitutions that control the chemical changes experienced by
370 tourmaline during the crystallization of this pegmatite, different binary composition
371 diagrams have been used (Fig. 7). At the beginning of the crystallization, the
372 compositional changes observed in tourmaline may be mainly explained by the
373 combination of two main mechanisms. The simple homovalent substitution FeMg_{-1} was
374 significantly operative for the tourmalines from the WZ (Fig. 7a). Starting from a
375 dravite-rich composition, this mechanism proceeded until the crystallization of the
376 intermediate zones, where tourmaline is mainly schorl, with a high content of vacancies
377 in the X-site. Parallel to the increase in Fe, tourmaline from the WZ becomes richer in
378 Al too, via the combination of the alkali-defect substitution $\text{Al}[\text{X}]^{\text{X}}(\text{R}^{2+}\text{Na})_{-1}$ and the
379 proton-loss substitution $^{\text{Y}}\text{Al}^{\text{W}}\text{O}(\text{R}^{2+\text{W}}(\text{OH}))_{-1}$, (where $\text{R}^{2+} = \text{Fe}^{2+} + \text{Mg}^{2+} + \text{Mn}^{2+} +$
380 Zn^{2+}), (Fig. 7b). Tourmalines from the IZ tend to follow the alkali-defect vector (Fig.
381 7b), suggesting that this mechanism strongly controlled the chemical variation of the
382 tourmalines until the end of the crystallization of the intermediate zone, where the
383 foitite component in tourmalines is important. In the CM, tourmaline composition
384 evolves from schorl toward elbaite. In the plot of R^{2+} versus $\text{Al}+\text{Li}$ (Fig. 7c), there is a
385 good negative correlation, which indicates that during most of the crystallization of the
386 CM, the Li and Al may have been incorporated according to the substitution schorl-
387 elbaite ($^{\text{Y}}\text{Al}^{\text{Y}}\text{Li}^{\text{Y}}\text{R}^{2+}_{-2}$). Later, during the crystallization of the pods constituting the CZ,
388 the tourmaline composition evolved via the combination of the schorl-elbaite and the
389 elbaite-rossmanite ($[\text{X}]^{\text{Y}}\text{Al}_{0.5}^{\text{X}}\text{Na}_{-1}^{\text{Y}}\text{Li}_{0.5}$) vectors, together with the already cited proton
390 loss and alkali-deficient vectors; as reflected by the plot of $\text{Li}+\text{Na}$ versus Fe_{tot} (Fig. 7d).
391 The increase of vacancies in the X site of the tourmaline from the pods in the CZ is
392 probably related to the abundance of albite in the CM, which would cause a depletion of
393 Na in the system. Finally, the gemmy tourmalines from the pockets inside the CZ pods
394 show a clear deprotonation (Figs. 7d and e), following the elbaite-darrellhenryite
395 exchange vector ($^{\text{Y}}\text{Al}^{\text{W}}\text{O}_2^{\text{Y}}\text{Li}_{-1}^{\text{W}}(\text{OH})_{-2}$). This substitution may reflect an increase in
396 oxygen fugacity, or a decrease in Li and F related to the crystallization of lepidolite and
397 amblygonite-montebrazite in the CZ adjacent to or within the pockets.

398

399 **Chemical Zoning**

400 In order to establish the pattern of the chemical zoning inside individual tourmaline
401 crystals, analyses were made across nine representative samples from the different

402 zones recognized in the Berry-Havey pegmatite. Results are plotted in Fig. 8, with the
403 exception of three samples that resulted to be very homogeneous. Main chemical
404 variations found in individual tourmaline crystals from the WZ correspond to Fe, Mg,
405 Al, and F, with slighter changes in Na and Ti (Fig. 8a). Profiles show a comb shape,
406 reflecting the texture of the crystals. Trends for Fe and Al are comparable and opposite
407 to those of Mg and F (Fig. 8a), whereas the Ca contents remain mainly constant. The
408 behavior of these elements is mainly consistent with the substitution schemes proposed
409 for the tourmalines in the WZ, i.e., the schorl-dravite and the proton-loss, with lower
410 influence of the alkali-deficient substitution (Fig. 8a). The prominent growth zoning
411 observed in some of the crystals from the WZ, less common in the inner parts of the
412 pegmatite, could be explained by an initial opening of the system along its contacts to
413 an influx of wall-rock derived components, as suggested by London & Manning (1995)
414 for tourmalines from Southwest England.

415 In the IZ most of the crystals appear homogeneous in backscattered electron
416 images, in contrast with those crystals from the WZ. Rarely, tourmaline crystals from
417 the IZ-I show irregular overgrowths (Fig. 8b). Accordingly, shapes of the compositional
418 trends resemble a plateau with a sharp transition toward the overgrowth. Contents in Fe
419 decrease suddenly in the overgrowths; whereas Al, Na and F show an opposite trend
420 (Fig. 8b). In the IZ-II tourmaline always occurs as big prismatic homogeneous crystals.
421 Tourmaline from the CM appears in a few different ways. The big black tapered prisms
422 that occur crowned by a pseudographic intergrowth of tourmaline + quartz \pm albite, are
423 usually homogeneous in BSE. Microprobe analyses across one of these prisms establish
424 their homogeneity. Crystals occurring in the crowns around the tapered prisms are more
425 heterogeneous, mainly in the case of coexistence of black and greenish or bluish
426 tourmaline (Figs. 8c, d, and e). When only black tourmaline is present in the crowns,
427 different well defined concentric zones occur, with a decrease in the Fe content toward
428 the rim, parallel to an increase in the Al, Na and F content (Fig. 8c). The chemical
429 composition across three different greenish portions of a crystal from one of the crowns
430 in the CM is plotted in Figs. 8d and e. The trends shown by Al, Na and F are, again,
431 quite similar and opposite to that of Fe. In all these cases, chemical variation across the
432 crystals from the CM seems to reflect the influence of the schorl-elbaite substitution,
433 operating during the crystallization of this zone.

434 Finally, in Fig. 8f it is possible to observe the chemical changes across a tourmaline
435 crystal from the vertical pegmatitic “branch” occurring to the south of the quarry. The

436 BSE image suggests a complex crystallization history, with cellular textures that
437 suggest a coalescence of small nuclei mantled by zones with patchy zoning, which
438 appears to represent stages of stabilization and destabilization of tourmaline. The
439 microprobe data reveal that the nuclei are Mg-Ca richer and Al-Fe-Na poorer than the
440 external zones (Fig. 8f). The tourmaline compositional changes are mainly described by
441 the $\text{AlNa}(\text{CaMg})_{-1}$ exchange vector, with a minor influence of the dravite-schorl
442 substitution. These are the Ca- and Mg-richest tourmalines analyzed in the Berry-
443 Havey pegmatite, which could reflect contamination by the calc-silicate country-rock. The
444 coalescence of a number of small grains, or crystallization centers, overgrown by outer
445 zones could indicate a relatively quick cooling along the “branch”.

446

447 **Chemical and textural changes in tourmaline and internal evolution of the Berry-** 448 **Havey pegmatite**

449 The Berry-Havey pegmatite shows a clear internal asymmetric zoning, where four
450 different units have been distinguished: wall zone, intermediate zone, core margin and
451 core zone. Tourmaline occurs in all these units, showing different textural features and
452 chemical composition for the distinct zones of the pegmatite. This way, tourmaline
453 becomes an important tool to interpret the crystallization history of its hosting rock.
454 Textural and chemical variations observed in tourmaline, from the WZ to the CZ,
455 suggest an inward fractional crystallization model. Despite the absence of the footwall
456 at the present level of exposure at the quarry, the asymmetry of the pegmatite and of the
457 distribution of tourmaline itself is evident, with the tapered tourmaline and the garnet
458 layers from the CM occurring only under the rare-element enriched zone. There is also
459 an important asymmetry between the proportions of the zones over and under the CZ,
460 with a clearly bigger volume for the IZ in the lower part. These asymmetries indicate
461 that the crystallization from the footwall and from the hanging-wall proceeded in a
462 different way. Further investigation would be necessary in order to explain the
463 development of such asymmetries.

464 Textures inside the pegmatite such as the quartz-K-feldspar and quartz-tourmaline
465 graphic intergrowths, and the comb tourmaline crystals, suggest that crystallization
466 proceeded under disequilibrium conditions from an undercooled melt (London 2008).
467 Crystallization of the tourmaline layer in the CM followed different steps. It starts with
468 the crystallization of the tapered prisms, in general perpendicular to the contacts. Then,
469 it follows with the formation of the crowns of quartz-tourmaline graphic intergrowth

470 around the tapered prisms, where the composition and color often change from black
471 schorl to greenish (or bluish) elbaite. Finally, it ends with the breaking of some of the
472 tourmaline crystals, mainly belonging to the crowns. The occurrence of an important
473 volume of tourmaline in this layer implies a significant depletion of B in the melt during
474 its crystallization. Some authors (e.g., Holtz et al. 1993, London, 2009) claim that the
475 presence of B₂O₃ enhances the solubility of water in the melt. Accordingly, the
476 formation of the tourmaline layer most probably lowered dramatically the solubility of
477 water in the remaining melt, which could lead to exsolution of a water-rich fluid. The
478 saturation in volatiles in the melt could be also favored by the previous crystallization of
479 important volumes of non-volatile components through anhydrous minerals, such as
480 quartz and feldspars, in the WZ and IZ of the pegmatite, which would have increased
481 the mole fraction of the volatile components in the melt. This way, the so-called
482 retrograde boiling of the fluid phase would occur, which most probably is related with
483 the formation of pockets. Assuming a closed system, we speculate that the breaking of
484 some of the last formed tourmaline crystals in the tourmaline layer of the CM could be
485 related to a sudden increase in the fluids pressure provoked by the exsolution of the
486 water-rich fluids from the melt, which imply a significant volume increase that could
487 cause brecciation (Phillips, 1973; Burnham & Ohmoto, 1980; Burnham, 1985). At this
488 point, the concentration of Fe was low enough and Li was high enough to allow the
489 crystallization of the first colored tourmalines in the CM, followed by the crystallization
490 of the CZ, where all the tourmaline corresponds to elbaite, with variable amounts of F,
491 Li, Al, Mn and vacancies. On the other hand, garnet crystallization ends in the CM,
492 below the CZ. This is most probably related to the increase of the Li and F content in
493 the pegmatite-forming system, which makes Mn compatible in micas and tourmaline.
494 This would destabilize garnet, whose composition had evolved to Mn-richer values
495 (Černý et al. 1985; London et al. 2001; London 2008).

496 As said above, the development of pockets inside the CZ was most probably related
497 to the exsolution of a fluid phase from the melt. The pockets represent the space that
498 was once filled by accumulated supercritical fluid (Nabelek et al. 2010, Simmons et al.,
499 2012), and show that the exsolved fluid was collected in discrete spaces instead of one
500 continuous space between the hanging and lower portions of the dikes (Maloney et al.
501 2008). Fluid inclusions in the quartz crystals from the pockets at the Berry-Havey are
502 mainly aqueous (Fuertes-Fuente, pers. com), which supports this model. Taking into
503 account the mineralogy of the pegmatite, the presence of pockets, and that the regional

504 metamorphism occurred at low pressure (Tomascak et al. 2005), we can assume that the
505 crystallization of the Berry-Havey pegmatite developed under pressures in the range 2-3
506 kb. The maximum water solubility in silicate melts at those pressures is ~6 wt. % in the
507 absence of boron (Holtz et al. 1995). This amount of H₂O, given its molar volume at
508 400°C and 2kbar, would occupy ~28% of the chamber volume (London, 2008; Maloney
509 et al. 2008). Based on these estimations, and on the relation between the volume of the
510 pockets and the volume of the CZ, it seems plausible that the exsolution of fluids from
511 the pegmatitic melt took place close to the end of the crystallization of the CM.
512 According to London (2008), the crystallization of granitic melt containing 6 wt. % H₂O
513 promotes a volume increase of 21% at constant pressure, and this release of vapor could
514 cause the rupture of the pegmatite. In our case, the rupture of the tourmaline crystals
515 close to the CZ and pockets therein.

516 The Li content increases gradually in tourmaline across the pegmatite, which
517 suggests that it was progressively enriched in the residual melt, due to its low solubility
518 in the minerals constituting the WZ and IZ (including mainly quartz, feldspars and
519 schorl) compared to its solubility in melt and fluid. According to Maloney et al. (2008)
520 concentrations in excess of 1 % Li₂O of the melts may be required for crystallization of
521 minerals in which Li is an essential structural constituent. Such high Li₂O
522 concentrations would have existed during the latest stages of crystallization of the CM
523 and during the crystallization of the CZ. However, a decrease in the Li and F contents is
524 observed in some of the tourmalines from the pockets, in comparison with the elbaite
525 from the pods of the CZ. This decrease could be related to the crystallization of late
526 lepidolite masses, growing in the pods close to the pockets, or inside the pockets. Also
527 the occurrence of rounded pods of amblygonite-montebasite in the CZ, some with
528 diameters >20 cm, would have sequestered a significant amount of Li and F, which
529 would be less available for the very latest tourmaline crystals, growing inside the
530 pockets.

531 Overall, the bulk composition of the Berry-Havey pegmatite is quite close to the
532 composition of a poorly evolved granitic melt. However, the most evolved facies,
533 occurring in the CZ, inside the pegmatite, are extremely enriched in incompatible
534 elements, mainly Li. This extreme enrichment in Li is reflected in the mineralogy of the
535 CZ, which includes lepidolite, elbaite and montebasite, as the main Li-bearing phases;
536 the three of them in important proportions. According to the classification of pegmatites
537 used lately (Černý and Ercit 2005), the mineralogy of the Berry-Havey would fit in the

538 complex type of the rare-element class belonging to the LCT family. There are two
539 different subtypes where this body could fit though: the lepidolite subtype and the
540 elbaite subtype. According to Novak and Povondra (1995), lepidolite subtype
541 pegmatites contain foitite as the most primitive tourmaline and rossmanite or (Fe-Mn)-
542 bearing elbaite as the most fractionated tourmaline, whereas elbaite subtype pegmatites
543 contain Mg-rich schorl as the most primitive, and elbaite or rarely liddicoatite as the
544 most fractionated tourmaline, which is the case of the Berry-Havey. Moreover, schorl in
545 the elbaite subtype is Na-rich, whereas in the lepidolite subtype it is rich in X-site
546 vacancies (Selway et al. 1999). According to these criteria, the Berry-Havey would
547 belong to the elbaite subtype. However, in the elbaite subtype the dominant Li-bearing
548 phase is elbaite and lepidolite is supposed to be accessory or absent (Novak and
549 Povondra 1995), which does not fit with the Berry-Havey body, where lepidolite is a
550 common mineral in the CZ. Therefore, we can conclude that the limit between these
551 two subtypes cannot be clearly delineated just by the composition of the minerals or by
552 their proportions.

553 **Implications**

554 Textural and paragenetic relations, as well as geochemical data outlined above,
555 highlight the importance of tourmaline as petrogenetic probe. Both, texture and
556 composition change progressively as crystal fractionation proceeds during the inward
557 crystallization of the pegmatite. Crystallization of other minerals, such as plagioclase,
558 micas and phosphates, has a strong influence on the chemistry of tourmaline. This is
559 particularly notorious for the tourmaline from the CZ, richer in vacancies in the X-site,
560 probably due to the crystallization of abundant albite in the CM, which reduced the
561 availability of Na in the final stage of tourmaline formation. Also the composition of
562 tourmaline from the pockets, deprotonated and poorer in Li and F, probably reflects the
563 influence of the crystallization of important amounts of lepidolite and amblygonite-
564 montebrasite in the CZ. The influence of the crystallization of tourmaline on the internal
565 evolution of the pegmatite is also evident, mainly in the case of the tourmaline layer
566 occurring under the core zone. The sudden depletion of B in the melt would have
567 lowered the water solubility, provoking the exsolution of a fluid phase, what is directly
568 related to the formation of pockets.

569 The content of trace elements in tourmaline associated to pegmatitic environments
570 is quite low in general, independently of the degree of fractionation of the facies where

571 this mineral appears. However, some elements, such as Li, Be, Mn, Nb, Ta and Sn,
572 present a progressive change parallel to fractionation.

573 Therefore, the study of the textural features and the chemical composition of
574 tourmaline is highly valuable for the understanding of the rocks where it occurs.

575

576

Acknowledgements

577 The authors thank Arnaud Villaros, Darrell Henry and David London for thorough
578 reviews and comments that have greatly helped to improve the manuscript. Authors are
579 also greatly indebted to Jeff Morrison, the owner of the Havey Quarry, who has always
580 facilitated the access to the pegmatite. Moreover, he and Ray Sprague, miner and
581 organizer of the Maine Pegmatite Workshop, have helped us during the collecting of the
582 samples, and kept us informed about all details in the pegmatite as they were mining it,
583 even providing clarifying pictures when necessary. This research has been financially
584 supported by the Spanish Ministerio de Economía y Competitividad (Project CGL2012-
585 31356, with ERDF funds) and by the CICYT (project CGL2009-12677). Also the
586 University of the Basque Country UPV/EHU contributed economically with the grant
587 GIU/1216.

588

589

References cited

- 590 Brown, M., and Solar, G.S. (1998a) Granite ascent and emplacement during contractional deformation in
591 convergent orogens. *Journal of Structural Geology*, 20(9/10), 1365-1393.
592 -. (1998b) Shear-zone systems and melts: feedback relations and self-organization in orogenic belts.
593 *Journal of Structural Geology*, 20(2/3), 211-227.
594 -. (1999) The mechanism of ascent and emplacement of granite magma during transpression: a
595 syntectonic granite paradigm. *Tectonophysics*, 312, 1-33.
596 Burnham, C. W. (1985) Energy release in subvolcanic environments: Implications for breccia formation.
597 *Economic Geology*, Vol. 80, p 1515 - 1522.
598 Burnham, C.W. & Ohmoto, H. (1980) Late-stage processes of felsic magmatism. *Mining Geology*
599 *Special Issue 8*, 1-11.
600 Čerňý, P., and Ercit, T.S. (2005) The classification of granitic pegmatites revisited. *Canadian*
601 *Mineralogist*, 43, 2005-2026.
602 Čerňý, P., Meintzer, R.E., and Anderson, A.J. (1985) Extreme fractionation in rare-element granitic
603 pegmatites; selected examples of data and mechanisms. *Canadian Mineralogist*, 23(3), 381-421.
604 De Yoreo, J.J., Lux, D.R., and Guidotti, C.V. (1991) Thermal modelling in low-pressure=high-
605 temperature metamorphic belts. *Tectonophysics*, 188(209-238).
606 Guidotti, C.V. (1989) Metamorphism in Maine: an overview. In R.D. Tucker, and R.G. Marvinney, Eds.
607 *Studies in Maine Geology*. 3, p. 1-19. Maine Geological Survey, Augusta, Maine.
608 -. (1993) H₂O solubility in haplogranitic melts; compositional, pressure, and temperature dependence.
609 *Geological Society of America, Northeastern Section Meeting, Abstracts with Programs*, 25,
610 A21.
611 Henry, D.J., and Dutrow, B.L. (1996) Metamorphic tourmaline and its petrologic applications. In: Grew
612 E. S. & Anovitz L. M. (eds.), *Boron: mineralogy, petrology and geochemistry. Reviews in*
613 *Mineralogy*, vol. 33, Mineralogical Society of America, 503-557.
614 Henry, D.J., Novak, M., Hawthorne, F.C., Ertl, A., Dutrow, B.L., Uher, P., and Pezzotta, F. (2011)
615 *Nomenclature of the tourmaline-supergroup minerals. American Mineralogist*, 96(5-6), 895-913.
616 Holtz, F., Behrens, H., Dingwell, D.B., and Johannes, W. (1995) H₂O solubility in haplogranitic melts;
617 compositional, pressure, and temperature dependence. *American Mineralogist*, 80, 94-108.
618 Holtz, F., Dingwell, D.B., and Behrens, H. (1993) Effects of F, B₂O₃ and P₂O₅ on the solubility of water
619 in haplogranite melts compared to natural silicate melts. *Contributions to Mineralogy and*
620 *Petrology*, 113, 492-501.

- 621 Johnson, T.E., Brown, M., and Solar, G.S. (2003) Low-pressure subsolidus and suprasolidus phase
622 equilibria in the MnNCKFMASH system. Constraints on conditions of regional metamorphism
623 in western Maine, northern Appalachians. *American Mineralogist*, 88, 624-638.
- 624 Jolliff, B.L., Papike, J.J., and Laul, J.C. (1986a) Mineral recorders of pegmatite internal evolution; REE
625 contents of tourmaline Geological Society of America, 99th annual meeting 18(6), 649.
- 626 Jolliff, B.L., Papike, J.J., and Shearer, C.K. (1986b) Tourmaline as a recorder of pegmatite evolution; Bob
627 Ingersoll Pegmatite, Black Hills, South Dakota. *American Mineralogist*, 71(3-4), 472-500.
- 628 Keller, P., Robles, E.R., Perez, A.P., and Fontan, F. (1999) Chemistry, paragenesis and significance of
629 tourmaline in pegmatites of the Southern Tin Belt, central Namibia. *Chemical Geology*, 158(3-
630 4), 203-225.
- 631 London, D. (2008) Pegmatites. *The Canadian Mineralogist*, Special Publication n° 10, 347.
- 632 London, D. (2009) The Origin of Primary Textures in Granitic Pegmatites. *The Canadian Mineralogist*,
633 47(4), 697-724.
- 634 London, D., Evensen, J.M., Fritz, E., Icenhower, J.P., Morgan VI, G.B., and Wolf, M.B. (2001)
635 Enrichment and accommodation of manganese in granite-pegmatite systems. *Geochimica Et*
636 *Cosmochimica Acta*, Eleventh Annual V. M. Goldschmidt Conference, May 20-24, 2001, Hot
637 Springs, Virginia. Abstract n° 3369.
- 638 London, D., and Manning, D.A.C. (1995) Chemical Variation and Significance of Tourmaline from
639 Southwest England. *Economic Geology and the Bulletin of the Society of Economic Geologists*,
640 90(3), 495-519.
- 641 Maloney, J.S., Nabelek, P.I., Sirbescu, M.L.C., and Halama, R. (2008) Lithium and its isotopes in
642 tourmaline as indicators of the crystallization process in the San Diego County pegmatites,
643 California, USA. *European Journal of Mineralogy*, 20(5), 905-916.
- 644 Nabelek, P.I., Whittington, A.G., and Hofmeister, A.M. (2010) The role of H₂O in rapid emplacement
645 and crystallization of granite pegmatites: resolving the paradox of large crystals in highly
646 undercooled melts. *Contributions to Mineralogy and Petrology*, 160, 313-325.
- 647 Nicholson, S.W., Dicken, C.L., Horton, J.D., Foose, M.P., Mueller, J.A.L., and Hon, R. (2006)
648 Preliminary integrated geologic map databases for the United States: Connecticut, Maine,
649 Massachusetts, New Hampshire, New Jersey, Rhode Island and Vermont. USGS Open-File
650 Report: 2006-1272.
- 651 Novak, M. (2000) Compositional pathways of tourmaline evolution during primary (magmatic)
652 crystallization in complex (Li) pegmatites of the Moldanubicum, Czech Republic *Mineralogy*
653 *and petrology of shallow depth pegmatites; papers from the First international workshop* 30(1),
654 45-56.
- 655 Novak, M., and Povondra, P. (1995) Elbaite Pegmatites in the Moldanubicum - a New Subtype of the
656 Rare-Element Class. *Mineralogy and Petrology*, 55(1-3), 159-176.
- 657 Osberg, P.H. (1978) Synthesis of the geology of the northeast Appalachians, U.S.A. In P.E. Schenk, and
658 E.T. Tosier, Eds. *Appalachian-Caledonide orogen*. Geological Survey of Canada, Paper 78-13,
659 p. 137-167.
- 660 Osberg, P.H., Hussey, A.M.I., and Boone, G.H. (1985) Bedrock Geologic Map of Maine. Maine
661 Geological Survey, 1:500,000 scale map.
- 662 Phillips, W. J. (1973) Mechanical effects of retrograde boiling and its probable importance in the
663 formation of some porphyry ore deposits. *Transactions Inst. Mining and Metallurgy (section B:*
664 *Appl. Earth Sci.)*. Printed in England, p. B90 - 98.
- 665 Pouchou, J.L., and Pichoir, F. (1985) "PAP" $\phi(\rho z)$ procedure for improved quantitative microanalysis. In
666 J.T. Armstrong, Ed. *Microbeam Analysis*, p. 104-106. San Francisco Press.
- 667 Roda, E., Pesquera, A., and Velasco, F. (1995) Tourmaline in Granitic Pegmatites and Their Country
668 Rocks, Fregeneda Area, Salamanca, Spain. *Canadian Mineralogist*, 33, 835-848.
- 669 Roda-Robles, E., Pesquera, A., Gil, P.P., Torres-Ruiz, J., and Fontan, F. (2004) Tourmaline from the rare-
670 element Pinilla pegmatite, (Central Iberian Zone, Zamora, Spain): chemical variation and
671 implications for pegmatitic evolution. *Mineralogy and Petrology*, 81(3-4), 249-263.
- 672 Roda-Robles, E., Pesquera, A., Gil-Crespo, P.P., and Torres-Ruiz, J. (2012) From granites to highly
673 evolved pegmatites: a case study of the Pinilla de Femoselle granite-pegmatite system (Zamora,
674 Spain). *Lithos*, 153, 192-207.
- 675 Roda-Robles, E., Simmons, W., Nizamoff, J., Pesquera, A., Gil-Crespo, P.P., and Torres-Ruiz, J. (2011)
676 Chemical variation in tourmaline from the Berry-Havey Pegmatite (Maine, USA), and
677 implications for pegmatitic evolution. *Asociación Geológica Argentina, Serie D, Publicación*
678 *Especial*, 14.
- 679 Selway, J.B., Novak, M., Cerny, P., and Hawthorne, F.C. (1999) Compositional evolution of tourmaline
680 in lepidolite-subtype pegmatites. *European Journal of Mineralogy*, 11(3), 569-584.

- 681 Simmons, W.B., Pezzotta, F., Shigley, J.E., and Beurlen, H. (2012) Granitic Pegmatites as Sources of
682 Colored Gemstones. *Elements*, 8, 281-287.
- 683 Solar, G.S., and Brown, M. (2001a) Deformation partitioning during transpression in response to Early
684 Devonian oblique convergence, northern Appalachian orogen, USA. *Journal of Structural*
685 *Geology*, 23, 1043-1065.
- 686 -. (2001b) Petrogenesis of Migmatites in Maine, USA: Possible Source of Peraluminous Leucogranite in
687 Plutons? *Journal of Petrology*, 42(4), 789-823.
- 688 Solar, G.S., and Tomascak, P.B. (2001) Is there a relation between transpressive deformation and pluton
689 emplacement in southern Maine? Geological Society of America, Abstracts with Programs, 33.
- 690 -. (2009) The Sebago Pluton and the Sebago Migmatite Domain, southern Maine; results from new
691 studies. 2009 Annual Meeting of Northeastern Section, Geological Society of America, Field
692 Trip 2, 1-24.
- 693 Tindle, A.G., Breaks, F.W., and Selway, J.B. (2002) Tourmaline in petalite-subtype granitic pegmatites:
694 Evidence of fractionation and contamination from the Pakeagama Lake and Separation Lake
695 areas of northwestern Ontario, Canada. *Canadian Mineralogist*, 40, 753-788.
- 696 Tomascak, P.B., Brown, M., Solar, G.B., Becker, H.J., Centorbi, T.L., and Tian, J. (2005) Source
697 contributions to Devonian granite magmatism near the Laurentian border, New Hampshire and
698 western Maine, USA. *Lithos*, 80, 75-99.
- 699 Tomascak, P.B., Krogstad, E.J., and Walker, R.J. (1996a) Nature of the crust in Maine, USA: evidence
700 from the Sebago batholith. *Contributions to Mineralogy and Petrology*, 125, 45-59.
- 701 -. (1996b) U-Pb monazite geochronology of granitic rocks from Maine: implications for late Paleozoic
702 tectonics in the northern Appalachians. *Journal of Geology*, 104, 185-195.
- 703 Wise, M.A., and Brown, C.D. (2010) Mineral chemistry, petrology and geochemistry of the Sebago
704 granite-pegmatite system, southern Maine, USA. *Journal of Geosciences*, 55(1), 3-26.
- 705
706
707

FIGURE CAPTIONS

708

709

710 Figure 1: a) Map showing the location of the Sebago Migmatite Domain in New
711 England and b) principal geological features of the area and location of the Berry-Havey
712 pegmatite.

713

714 Figure 2: Schematic map and cross sections of the Berry-Havey pegmatite.

715

716 Figure 3: BSE images of: a) tourmaline crystals from the WZ showing successive
717 overgrowths, with finger-like shapes pointing toward the inner parts of the pegmatite; b)
718 tourmaline crystal from the IZ-I, partially rimmed by discontinuous thin zones of
719 different brightness; c) tourmaline prism from the CM showing a homogeneous core,
720 surrounded by a concentric rim with a different color, that is overgrown by a much
721 thinner, darker, frayed edge; d) greenish area in a tourmaline crystal from the CM
722 showing patchy zoning or cellular textures in the inner zones of the crystals, which are
723 overgrown by darker rims; and, e) tourmaline crystal from a vertical pegmatitic
724 “branch”, including more than one tiny nucleus that appears overgrown by lighter
725 zones, which may account for coalescence of small grains mantled by outer zones with
726 a very irregular shape.

727

728 Figure 4: a) black, prismatic crystals of schorl from the IZ-II; b) Thick ends of tapered
729 prisms of tourmaline, crowned by black tourmaline, intergrown with quartz ± albite
730 (cleavelandite), giving a graphic texture in the CM; c) black tourmaline crystal rimmed
731 by greenish tourmaline, with a sharp transition from black to colored tourmaline in the
732 CM; d) radial prisms of multicolored tourmaline embedded in feldspars and quartz from
733 the pods of the CZ; e) euhedral to subhedral greenish gem-quality tourmaline crystals
734 from a pocket in the CZ; and, f) greenish and purple radial prismatic tourmaline crystal,
735 laying over a clay-minerals bed, from a pocket in the CZ.

736

737 Figure 5: Plots of the chemical composition of tourmalines from the different units in
738 the Berry-Havey pegmatite: a) X-site plot of (Na + K) - Ca - X-site vacancy; b) variation
739 in

740 $R^{2+}/R^{2+}+2Li$ versus $\square/(\square+Na+K)$ as proposed by Henry et al. (2011) for the
741 classification of tourmaline; c) triangular plot of Li - Al(Y) - Fe+Mn; and, d) X-site
742 charge versus F. All data in apfu.

743

744 Figure 6: Box and whisker plots for the trace elements in tourmaline from the different
745 units in the Berry-Havey pegmatite.

746

747 Figure 7: a) Mg versus Fe (total); b) Al versus \square (X-site vacancies); c) R^{2+} versus
748 Al+Li; d) Fe (total) versus Li+Na; and, e) Al(Y)- \square versus $R^{2+}+\square$. The directions of
749 some selected exchange-vectors are shown for reference.

750

751 Figure 8: Representative chemical zoning patterns for tourmaline, and their correspondence to the BSE
752 image. a) Wall zone, b) Intermediate zone-I, c) black crystal from the tourmaline crowns in the core
753 margin, d and e) Greenish crystals from the tourmaline crowns in the core margin, and f) vertical
754 pegmatitic “branch”.

755

756

757

TABLE CAPTIONS

758

759

760 Table 1: Main characteristics of the Berry-Havey pegmatite units and the associated
761 tourmaline

762

763 Table 2: Representative microprobe analyses of tourmaline from the different units in
764 the Berry-Havey pegmatite.

765

766 Table 3: Representative LA-ICP-MS analyses of tourmaline from the different units in
767 the Berry-Havey pegmatite.

768

769

Table 1. Main characteristics of the Berry-Havey pegmatite units and the associated tourmaline

ZONE	MINERALOGY	GENERAL TEXTURES	TOURMALINE TEXTURE	TOURMALINE COMPOSITIONAL VARIATION
Wall	Qz, Kfs, Pl, Bt, Ms ± Grt ± black tourmaline	Homogeneous, very fine to medium grained facies. Locally greenish Kfs	Very fine grained, black prismatic crystals. Very scarce	Mg-rich Schorl- Schorl
Intermediate-I	Qz, Kfs ± Grt ± Bt ± black tourmaline	Qz-Kfs graphic intergrowths (> 90% volume)	Fine to medium subhedral crystals	Schorl-Foitite
Intermediate-II	Qz, Kfs, black tourmaline	Blocky Kfs and Qz	Coarse prismatic black crystals	Schorl-Foitite
Core margin	Ab, Qz, black ± green tourmaline	Matrix of tabular crystals of Clv, where coarse tourmaline crystals occur	Coarse black tourmaline prisms (< 70 cm length) crowned by an intergrowth of black±green Tur and Ab. Sharp contact between black and green tourmaline	From Schorl to Elbaite
Core Zone	Qz, Kfs, Lpd, Ms, Li-Ms, Amb, Ab, Brl, Fe-Mn Pho. Green, pink & multicolored tourmaline	Irregular pods of fine grained Lpd, coarse book Ms. Amb, Fe-Mn-Pho ± Cst± Col-Tan Coarse morganite (Brl) sub- to euhedral crystals are common. Sub-rounded pods of Fe-Mn-Pho or Amb Pockets with elbaite in a Cook matrix	In the pods, subhedral, fine to medium zoned crystals (watermelon, or longitudinal zoning). Also fine individual pink or green crystals (together with Lpd and Ms respectively) In the pockets, some green, teal or watermelon gem quality crystals	Pods: Elbaite-Rossmanite Pockets (gem): Elbaite-Rossmanite Olenite

In "Mineralogy", the following abbreviations have been used: Qz=quartz; Kfs=feldspar; Pl=plagioclase; Ms=moscovite; Bt=biotite; Grt=garnet; Tur=tourmaline; Ab=albite; Clv=cleavelandite; Amb=amblygonite-montebrazite; Cst=cassiterite; Col-Tan=columbite-tantalite; Lpd=lepidolite; Pho=phosphates; Brl=beryl; Cook=cookeite. *Grain size: very fine = <6 mm; fine = 6 mm to 2.5 cm; medium = 2.5 cm to 10 cm; coarse = >10 cm.

Anal. (#)	1	2	3
Zone^(a)	WZ	IZ	IZ
Color	Black	Black	Black
	oxy-dravite	oxy-schorl	schorl
SiO₂	36.30	35.62	35.35
TiO₂	0.75	0.15	0.29
Al₂O₃	33.23	33.72	33.35
Cr₂O₃	0.00	0.00	0.00
FeO(t)	7.43	12.53	13.12
MnO	0.08	0.00	0.20
MgO	5.54	1.42	1.84
ZnO	0.00	0.39	0.36
CaO	0.73	0.13	0.16
Na₂O	1.95	1.98	1.90
K₂O	0.05	0.05	0.04
Li₂O*	0.01	0.04	0.03
F	0.00	0.36	0.41
Cl	0.00	0.00	0.00
O=F	0.00	0.15	0.17
H₂O**	3.23	3.10	3.33

B₂O₃**	10.50	10.26	10.33
TOTAL**	99.79	99.62	100.52
Si	6.01	6.03	5.95
Al(IV)	0.00	0.00	0.05
B	3	3	3
Al(Z)	6.00	6.00	6.00
Al(Y)	0.48	0.73	0.57
Ti	0.09	0.02	0.04
Cr	0.00	0.00	0.00
Fe²⁺(t)	1.03	1.78	1.85
Mn	0.01	0.00	0.03
Mg	1.37	0.36	0.46
Zn	0.00	0.05	0.04
Li	0.01	0.03	0.02
Y	2.99	2.97	3.00
Ca	0.13	0.02	0.03
Na	0.63	0.65	0.62
K	0.01	0.01	0.01
X	0.77	0.69	0.66
□	0.23	0.31	0.34

F	0.00	0.19	0.22
Cl	0.00	0.00	0.00
O*	0.58	0.52	0.26
OH*	3.42	3.28	3.52
□/(□+Na)	0.27	0.33	0.35
Mg/(Mg+Fe)	0.57	0.17	0.20
Al (t)	6.48	6.73	6.62
Fe+Mg+Mn+Si	8.42	8.17	8.29

(a) WZ= Wall zone; IZ= Intermediate zone; CM =Core Margin zor

	5		6		7		8		9	
4	CMZ	Black	CMZ	Green	CMZ	Blue	CMZ	Multicoloured	CMZ	CZ
	oxy-schorl	schorl	fluor-schorl	fluor-schorl	fluor-elbaite	fluor-elbaite	fluor-elbaite	fluor-elbaite	fluor-elbaite	Watermelon fluor-elbaite
	35.39	34.67	36.18	36.18	37.49	37.49	38.34	38.34	38.30	38.30
	0.00	0.00	0.00	0.00	0.11	0.11	0.00	0.00	0.05	0.05
	33.43	33.86	35.25	35.25	37.07	37.07	39.86	39.86	39.54	39.54
	0.00	0.01	0.00	0.00	0.00	0.00	0.00	0.00	0.00	0.00
	13.76	14.86	10.44	10.44	5.21	5.21	1.43	1.43	1.68	1.68
	0.49	0.51	0.38	0.38	1.24	1.24	1.08	1.08	1.11	1.11
	0.00	0.00	0.00	0.00	0.00	0.00	0.00	0.00	0.00	0.00
	0.24	0.36	0.39	0.39	0.25	0.25	0.20	0.20	0.00	0.00
	0.13	0.01	0.06	0.06	0.11	0.11	0.29	0.29	0.33	0.33
	1.90	1.71	2.13	2.13	2.51	2.51	2.09	2.09	2.21	2.21
	0.14	0.03	0.02	0.02	0.00	0.00	0.00	0.00	0.03	0.03
	0.14	0.14	0.88	0.88	1.41	1.41	2.02	2.02	2.06	2.06
	0.56	0.71	0.99	0.99	0.95	0.95	1.12	1.12	1.42	1.42
	0.00	0.00	0.00	0.00	0.00	0.00	0.00	0.00	0.00	0.00
	0.24	0.30	0.42	0.42	0.40	0.40	0.47	0.47	0.60	0.60
	3.01	3.38	3.29	3.29	3.16	3.16	3.25	3.25	3.11	3.11

10.14	10.23	10.50	10.72	11.09	11.07
99.10	100.17	100.08	99.82	100.29	100.32
6.07	5.89	5.99	6.08	6.01	6.01
0.00	0.11	0.01	0.00	0.00	0.00
3	3	3	3	3	3
6.00	6.00	6.00	6.00	6.00	6.00
0.76	0.67	0.87	1.08	1.37	1.32
0.00	0.00	0.00	0.01	0.00	0.01
0.00	0.00	0.00	0.00	0.00	0.00
1.97	2.11	1.45	0.71	0.19	0.22
0.07	0.07	0.05	0.17	0.14	0.15
0.00	0.00	0.00	0.00	0.00	0.00
0.03	0.04	0.05	0.03	0.02	0.00
0.10	0.10	0.59	0.92	1.27	1.30
2.93	3.00	3.00	2.92	2.99	2.99
0.02	0.00	0.01	0.02	0.05	0.06
0.63	0.56	0.68	0.79	0.63	0.67
0.03	0.01	0.00	0.00	0.00	0.01
0.69	0.57	0.70	0.81	0.68	0.73
0.31	0.43	0.30	0.19	0.32	0.27

0.30	0.38	0.52	0.48	0.56	0.70
0.00	0.00	0.00	0.00	0.00	0.00
0.51	0.04	0.00	0.17	0.00	0.00
3.19	3.58	3.48	3.34	3.44	3.30
0.33	0.43	0.31	0.20	0.33	0.28
0.00	0.00	0.00	0.00	0.00	0.00
6.76	6.78	6.88	7.08	7.37	7.32
8.11	8.08	7.49	6.95	6.34	6.38

re; CZ= Core zone; CPZ= Core-pocket zone. * determined by Laser Ablation, ** calculated by

10	11	12	13
CZ	CZ	CZ	CPZ
Watermelon elbaita	Green fluor-elbaita	Pink fluor-elbaita	Green darrellhenryite
38.77	37.78	38.13	38.09
0.07	0.07	0.00	0.06
41.90	39.94	41.48	43.53
0.05	0.03	0.15	0.01
0.12	2.48	0.00	0.00
0.14	1.09	0.54	0.19
0.00	0.00	0.00	0.00
0.00	0.10	0.17	0.00
0.03	0.00	0.33	0.00
1.98	2.18	1.88	1.74
0.11	0.01	0.03	0.00
2.28	1.64	2.29	1.45
0.25	1.01	1.06	0.53
0.10	0.00	0.00	0.00
0.13	0.43	0.45	0.22
3.64	3.21	3.28	2.89

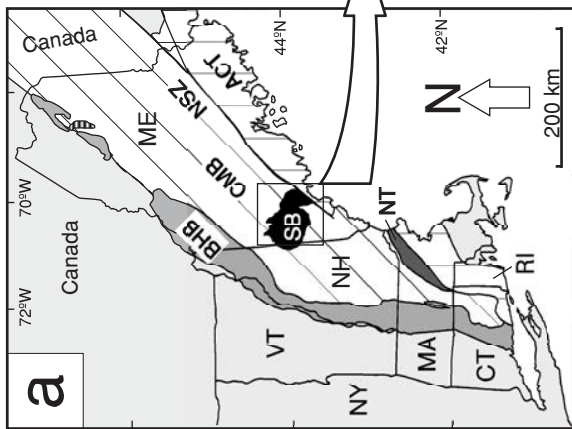
11.31	10.96	11.23	11.06
100.62	100.08	100.14	99.33
5.96	5.99	5.90	5.99
0.04	0.01	0.10	0.01
3	3	3	3
6.00	6.00	6.00	6.00
1.54	1.45	1.46	2.05
0.01	0.01	0.00	0.01
0.01	0.00	0.02	0.00
0.02	0.33	0.00	0.00
0.02	0.15	0.07	0.03
0.00	0.00	0.00	0.00
0.00	0.01	0.02	0.00
1.41	1.05	1.43	0.91
3.00	3.00	3.00	3.00
0.01	0.00	0.05	0.00
0.59	0.67	0.57	0.53
0.02	0.00	0.01	0.00
0.62	0.67	0.63	0.53
0.38	0.33	0.37	0.47

0.12	0.51	0.52	0.26
0.02	0.00	0.00	0.00
0.00	0.09	0.00	0.67
3.85	3.40	3.48	3.07
0.39	0.33	0.40	0.47
0.00	0.00	-	-
7.59	7.46	7.57	8.06
5.99	6.46	5.97	6.01

stoichiometry.

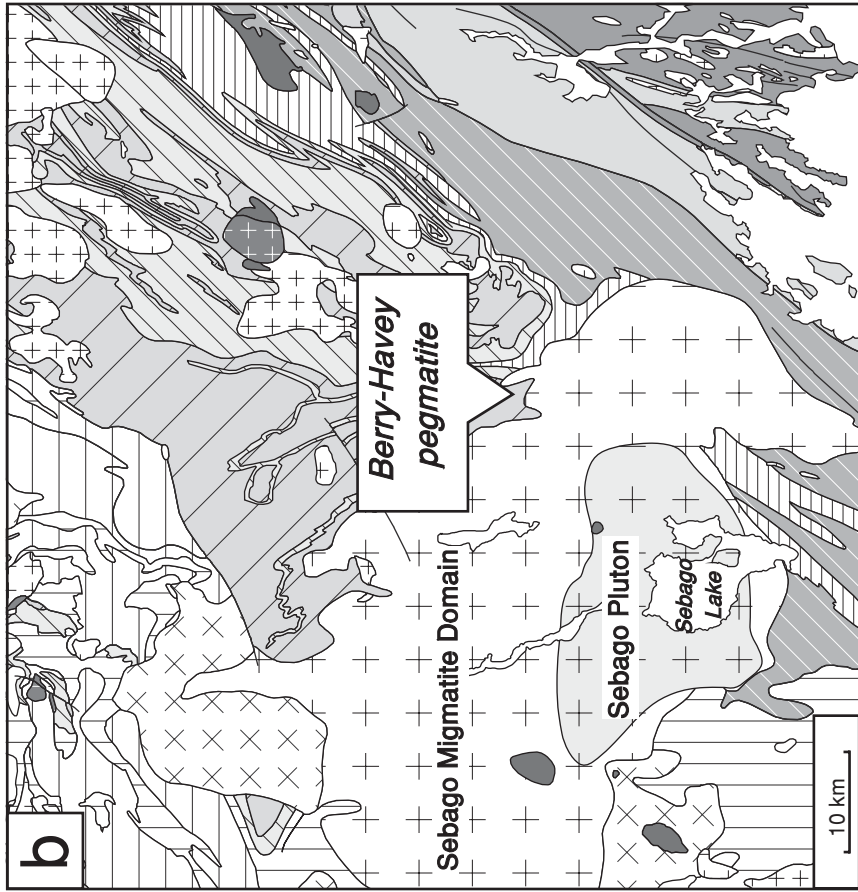
Anal. (#)	1	2	3	4	6	5	7	8	9
Zone ^(a)	WZ	IZ	IZ	CMZ	CMZ	CMZ	CZ	CZ	CPZ
Color	Black	Black	Black	Black	Green	Blue	Multicoloured	Pink	Green
Li	50.49	114.47	117.96	657.14	4087.53	5113.22	9734.64	11873.94	8373.45
Be	1.19	10.38	4.68	5.51	6.29	39.55	13.16	17.16	6.53
P	18.18	79.98	0.00	36.37	29.45	29646.56	18.58	0.00	0.00
Ca	0.70	0.13	0.13	0.05	0.08	9.86	0.36	0.37	0.00
Sc	47.05	10.04	5.06	0.93	3.29	1.28	2.14	1.96	4.03
V	15.96	0.45	0.70	0.41	0.55	0.58	0.52	0.62	0.00
Cr	5.48	0.80	0.00	0.00	0.45	0.85	0.00	0.00	0.00
Mn	282.13	1110.37	1462.96	4898.49	4516.56	11820.04	7671.91	6162.88	1479.06
Co	12.64	0.24	1.56	0.04	0.03	0.05	0.02	0.00	0.00
Ni	13.15	0.00	2.91	0.00	0.07	0.05	0.00	0.90	0.00
Cu	0.96	0.35	1.48	0.71	0.98	0.64	6.21	1.37	3.39
Zn	278.81	1640.29	1788.25	4889.43	4675.63	3528.29	1021.94	157.06	275.83
Ga	83.05	153.08	136.39	176.74	125.40	217.56	260.83	245.20	174.77
Rb	0.02	0.06	0.07	0.06	0.05	18.90	0.02	0.08	0.00
Sr	15.96	1.03	0.40	0.08	0.17	66.76	1.45	0.63	0.00
Y	0.08	0.00	0.03	0.01	0.00	0.01	0.02	0.01	0.23
Zr	0.31	0.10	0.13	0.02	0.06	18.36	0.05	0.07	0.44
Nb	0.24	1.17	1.89	1.15	0.75	1.43	4.96	6.70	1.44
Sn	8.01	20.53	16.65	53.90	40.56	49.31	94.98	148.85	47.84
Cs	0.00	0.00	0.01	0.00	0.04	11.94	0.00	0.15	0.10
Ba	0.04	0.01	0.11	0.01	0.09	7.69	0.01	0.52	0.16
La	3.69	0.32	0.78	0.01	0.01	0.00	0.61	0.07	0.00
Ce	6.15	0.42	1.41	0.00	0.00	0.01	1.09	0.00	0.00
Pr	0.42	0.03	0.13	0.00	0.00	0.00	0.08	0.01	0.10
Nd	1.22	0.09	0.24	0.01	0.10	0.04	0.24	0.00	0.00
Sm	0.20	0.00	0.00	0.01	0.00	0.00	0.20	0.12	0.00
Eu	0.11	0.00	0.00	0.01	0.01	0.01	0.02	0.01	0.00
Gd	0.10	0.06	0.00	0.01	0.07	0.04	0.01	0.00	0.40
Tb	0.01	0.00	0.00	0.00	0.01	0.01	0.00	0.00	0.00
Dy	0.04	0.00	0.00	0.00	0.04	0.00	0.00	0.00	0.58
Ho	0.00	0.00	0.00	0.00	0.00	0.00	0.00	0.00	0.00
Er	0.00	0.00	0.00	0.00	0.00	0.00	0.03	0.00	0.00
Tm	0.00	0.00	0.00	0.00	0.00	0.00	0.00	0.00	0.00
Yb	0.01	0.00	0.00	0.04	0.01	0.00	0.00	0.00	0.00
Lu	0.00	0.00	0.00	0.01	0.01	0.01	0.00	0.00	0.00
Hf	0.04	0.03	0.03	0.01	0.00	0.58	0.02	0.00	0.00
Ta	0.07	0.26	0.34	0.28	0.37	0.65	2.14	5.96	1.15
W	0.01	0.05	0.00	0.01	0.00	0.33	0.00	0.03	0.33
Tl	0.00	0.00	0.00	0.03	0.00	0.04	0.00	0.00	0.00
Pb	4.99	1.55	2.57	1.87	6.95	128.83	89.32	321.74	18.45
Th	0.00	0.00	0.01	0.00	0.02	0.01	0.07	0.26	0.26
U	0.00	0.01	0.00	0.01	0.02	12.03	0.02	0.02	0.00
LREE	11.68	0.86	2.57	0.04	0.11	0.05	2.22	0.20	0.10
LREE	0.26	0.06	0.00	0.06	0.16	0.07	0.05	0.01	0.98

(a) WZ= Wall zone; IZ= Intermediate zone; CM =Core Margin zone; CZ= Core zone; CPZ= Core-pocket zone.



- BHB** Bronson Hill Belt
- CMB** Central Maine Belt
- NSZ** Norumbega Shear Zone System
- NT** Nashoba Terrane
- ACT** Avalon Composite Terrane
- SB** Sebago Batholith

ME, Maine; NY, New York; VT, Vermont; NH, New Hampshire; MA, Massachusetts; CT, Connecticut; RI, Rhode Island.



Igneous Rocks

- Sebago Pluton
- Sebago Migmatite Domain
- Granodiorites and tonalites
- Syenites and quartz monzonites
- Gabbros
- Granites










Metamorphic and Sedimentary Rocks

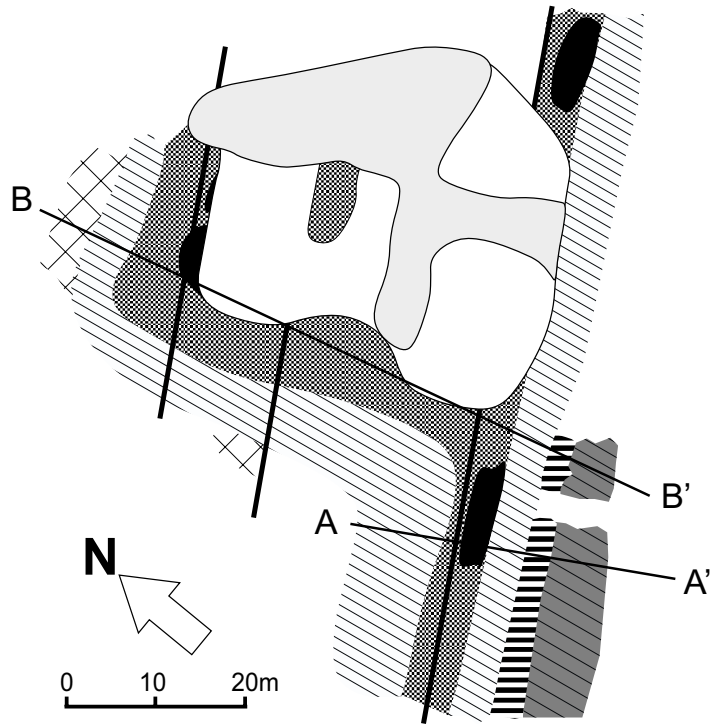
- Schists and metasedimentary rocks (Devonian)
- Shales, mudstones, quartzites, limestones and migmatites (Silurian-Devonian)
- Sandstones (Silurian)
- Marbles and metasedimentary rocks (Silurian)
- Slates and calc-silicate rocks (Silurian)
- Sandstones (Ordovician-Silurian)
- Metavolcanic rocks (Precambrian-Ordovician)
- Slates (Precambrian-Ordovician)

a: Modified from Brown and Solar (1998a)

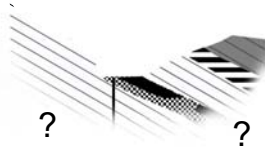
b: Modified from Osberg et al. (1985), Nicholson et al (2006), Wise and Brown (2010)

LEGEND

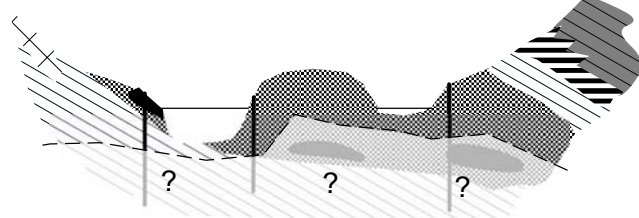
-  Dumps
-  Water
-  **Core Zone: Pockets**, multicolored tourmaline + Lep + Clay minerals
Pods, blocky Qtz + blocky Kfs + book Ms + lepidolite masses + phosphate pods (Amb + Fe-Mn) ± Brl (morg.) ± Cst ± Col-Tan
-  **Core margin**: Qtz + Clv + schorl suns with crown of graphic intergrowth (black ± green Tur)
-  **Intermediate-II**: prismatic coarse schorl crystals inside blocky Kfs and Qtz
-  **Intermediate-I**: Qtz + Kfs graphic intergrowth ± Grt ± Bt ± Tur (schorl)
-  **Wall Zone**: fine medium grained facies Qtz + Bt + Kfs + Ms ± Grt ± Tur
-  Metamorphic country rock (amphibolites)
-  Basalt dyke

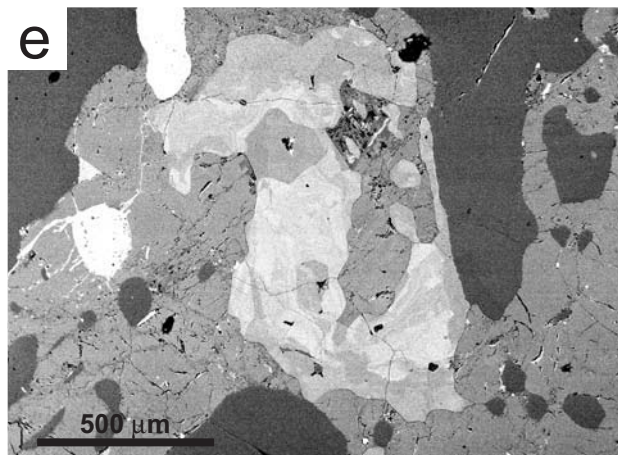
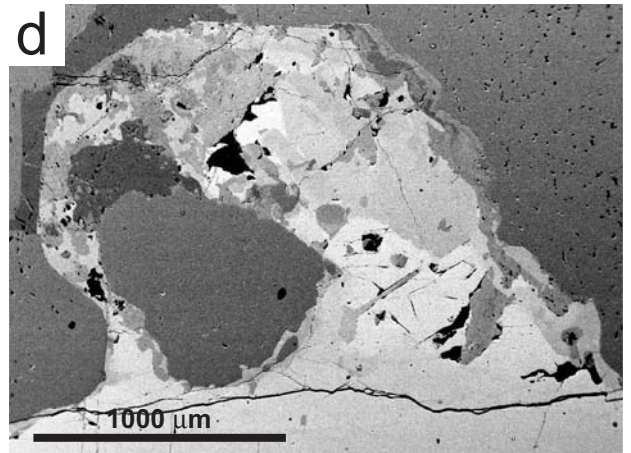
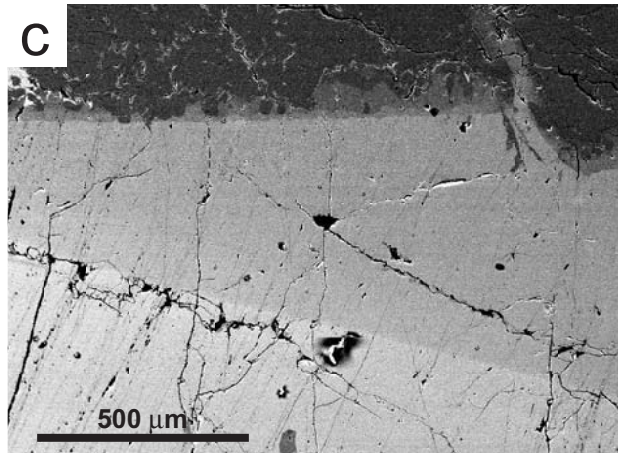
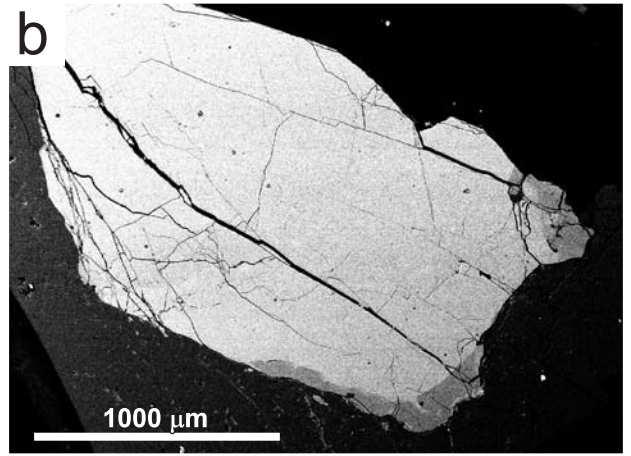
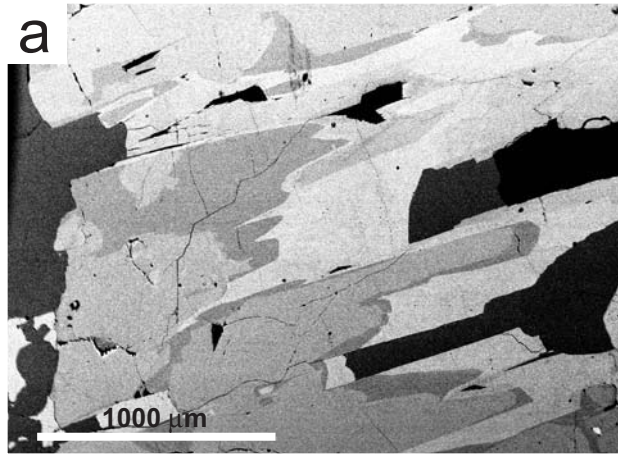


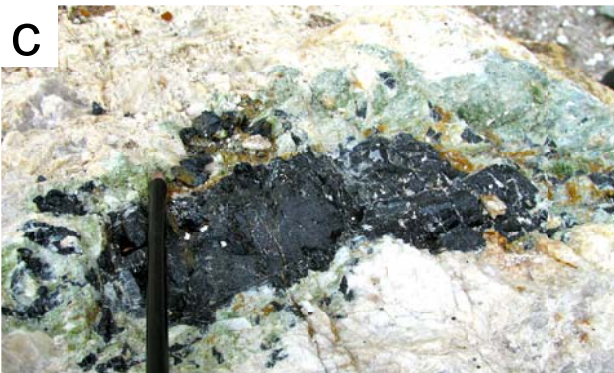
A ————— A'

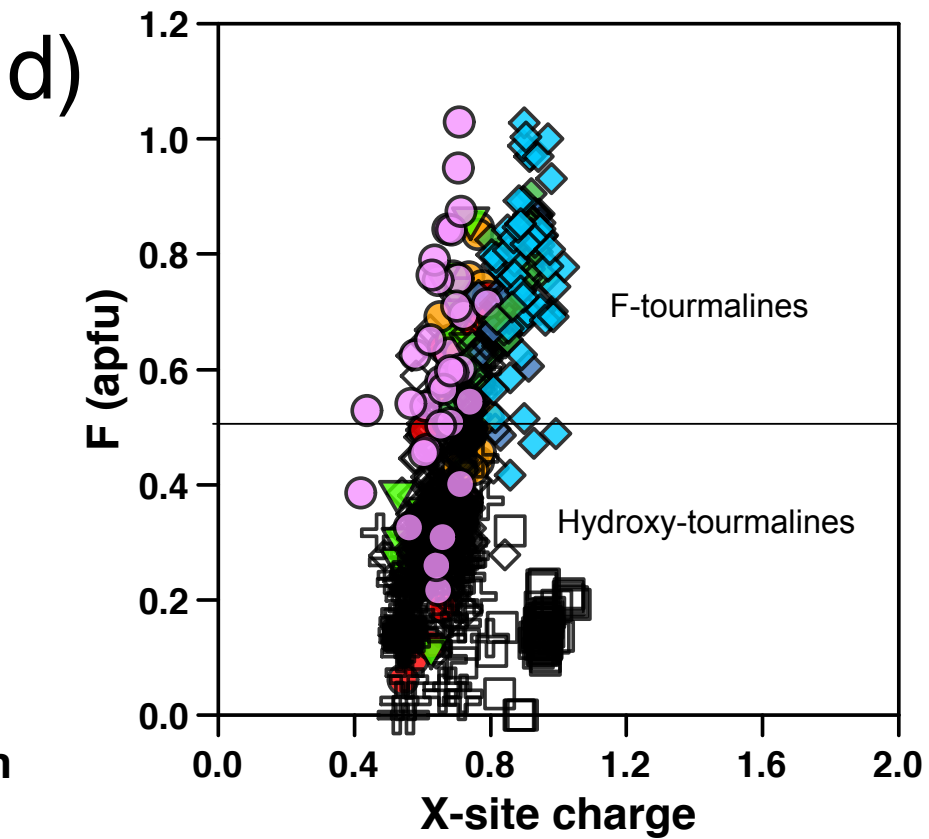
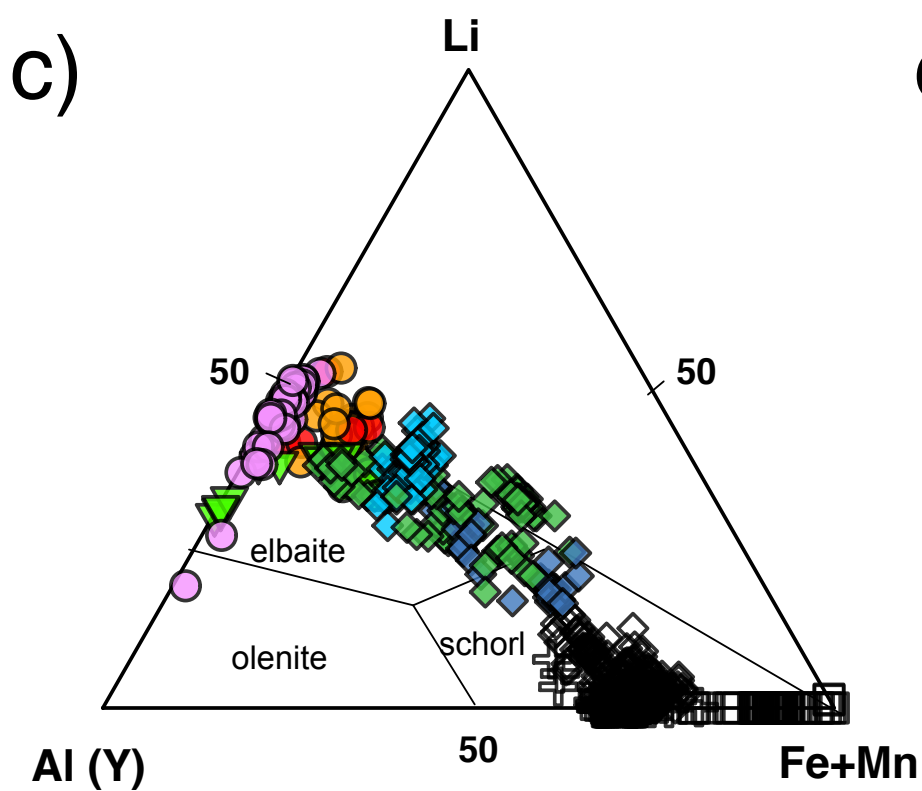
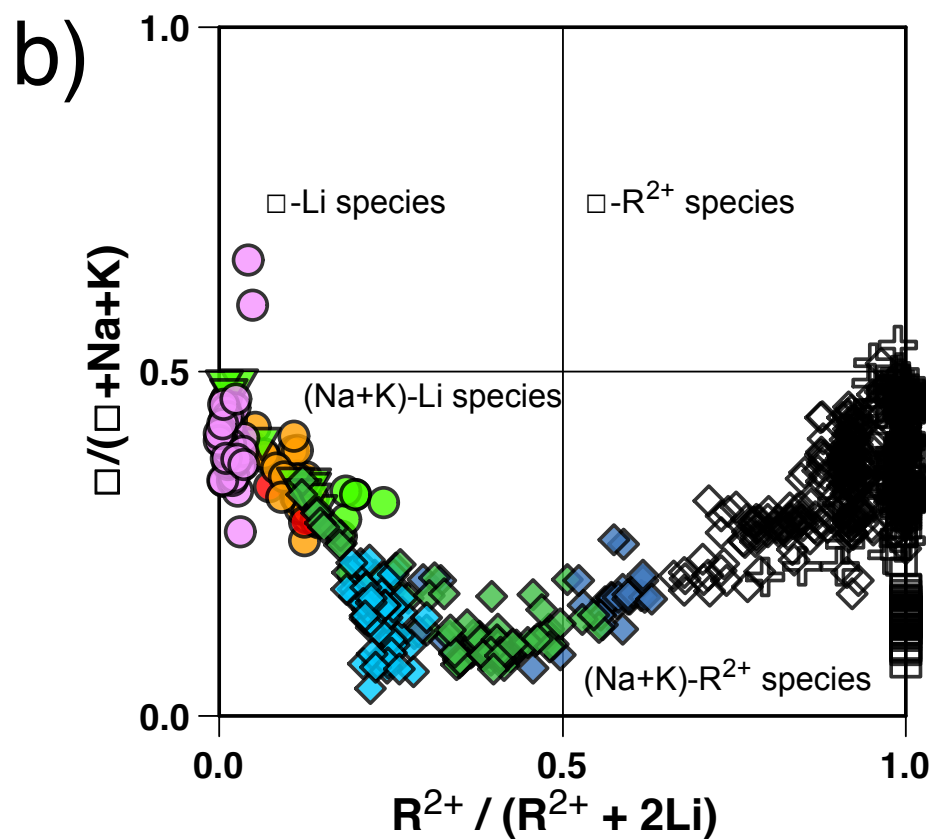
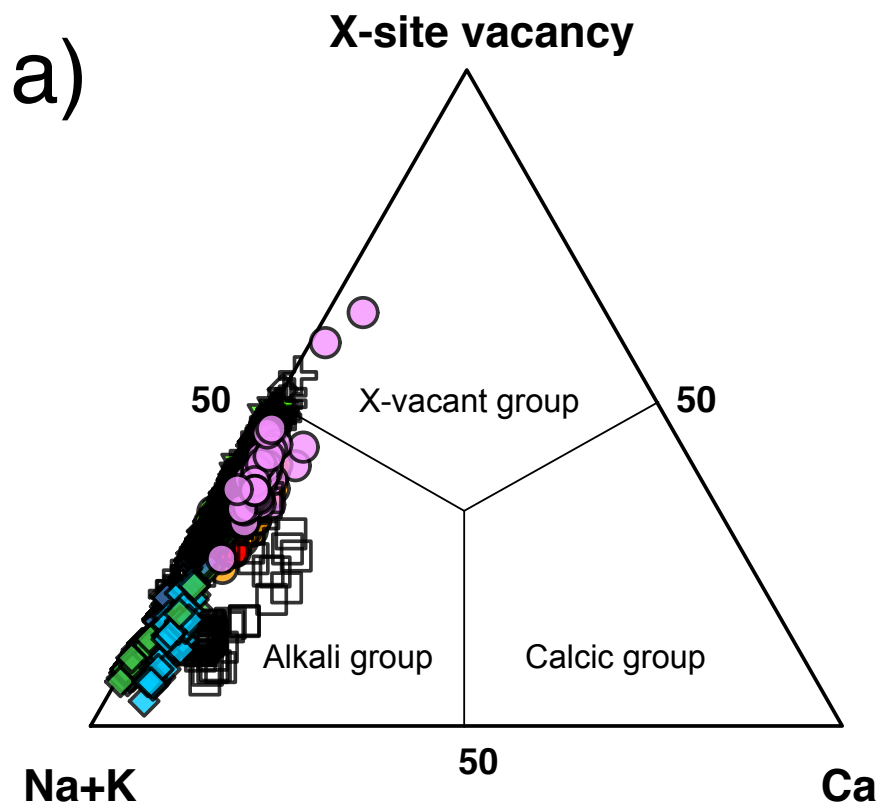


B ————— B'

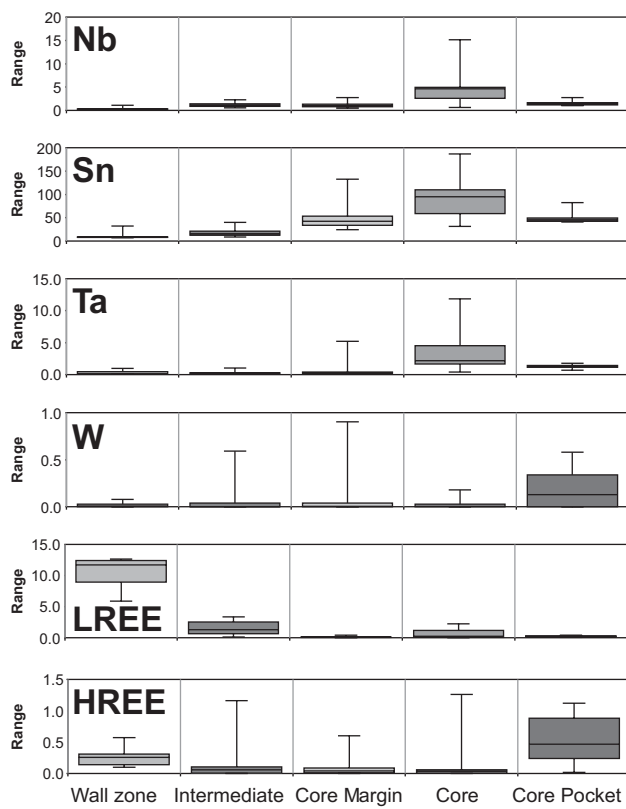
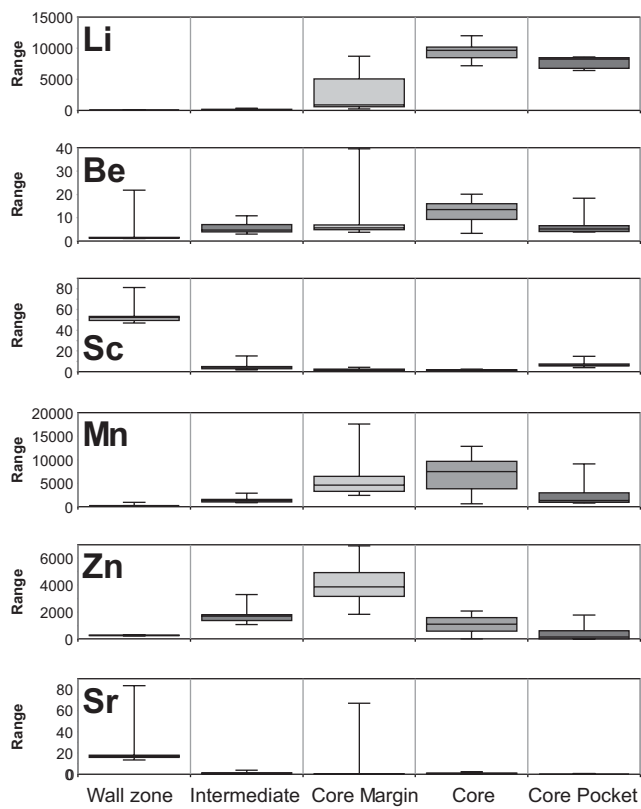


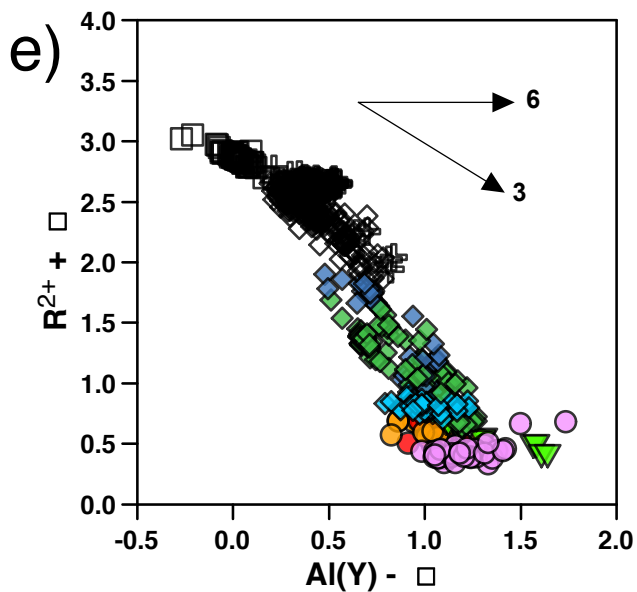
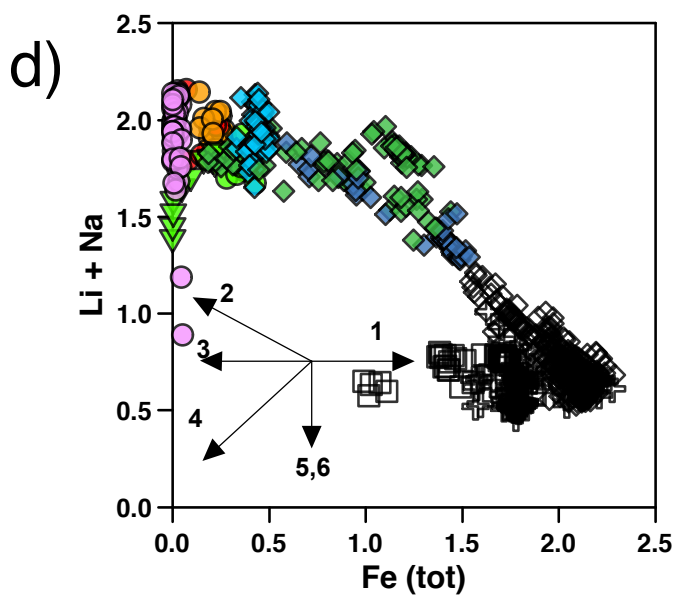
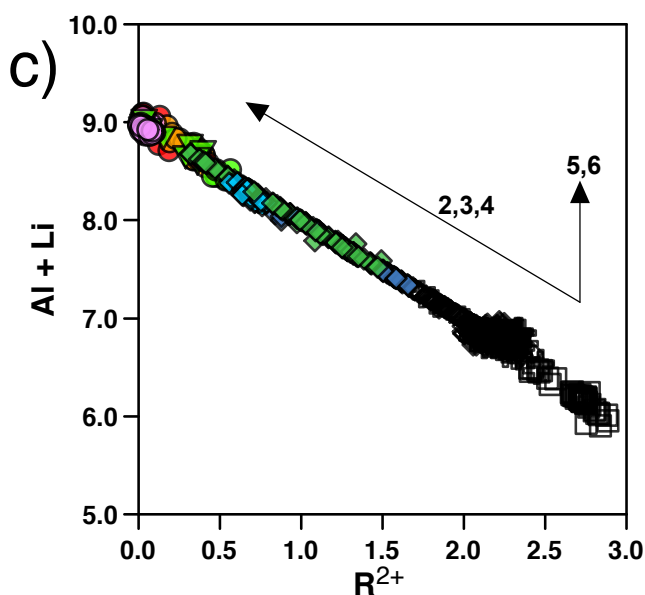
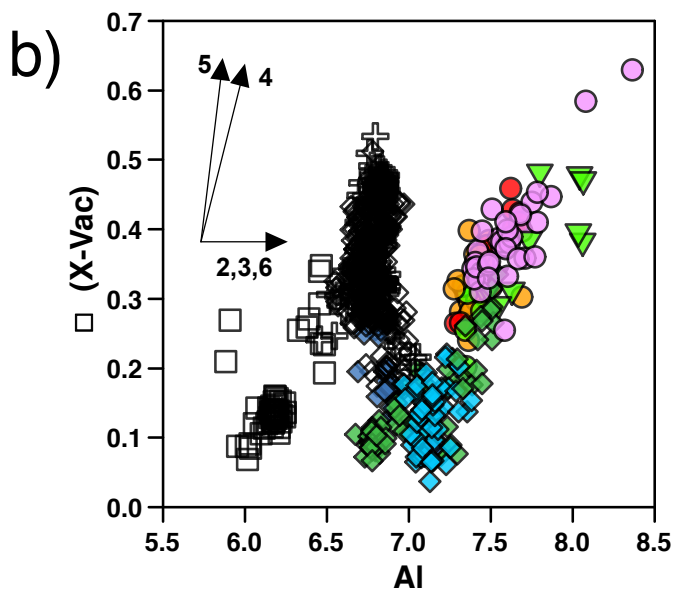
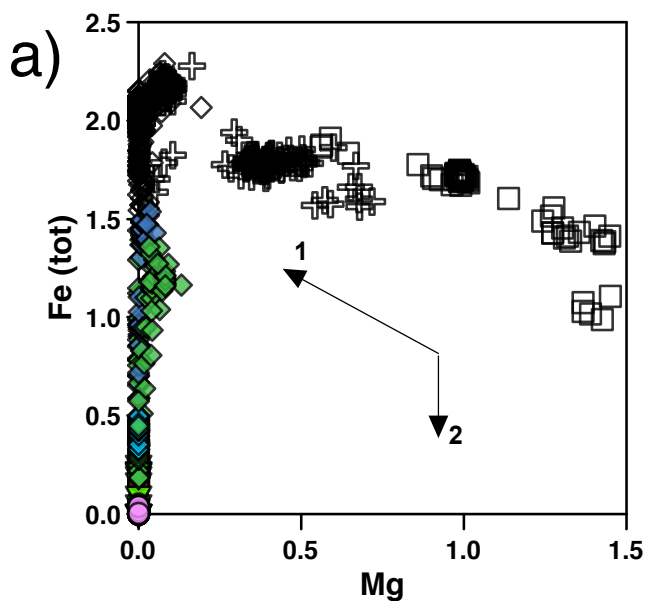






- Wall Zone
- ⊕ Intermediate Zone (back)
- ◇ Core Margin Zone (black)
- ◆ Core Margin Zone (green)
- ◆ Core Margin Zone (dark blue)
- ◆ Core Margin Zone (blue)
- Core Zone (watermelon)
- Core Zone (multicoloured)
- Core Zone (green)
- Core Zone (pink)
- ▼ Core-Pocket Zone (green)





- 1- Fe (Mg)_{-1}
- 2- $\text{Al Li Fe}^{2+}_{-2}$
- 3- $\text{Al O (R}^{2+} \text{ OH)}_{-1}$
- 4- $\text{Al } \square \text{ (R}^{2+} \text{ Na)}_{-1}$
- 5- $\square \text{ Al}_{0.5} \text{ Na}_{-1} \text{ Li}_{-0.5}$
- 6- $\text{Al O}_2 \text{ Li}_{-1} \text{ (OH)}_{-2}$

